International Journal of Adhesion & Adhesives 150 (2026) 104387

Contents lists available at ScienceDirect

International Journal of Adhesion and Adhesives

journal homepage: www.elsevier.com/locate/ijadhadh

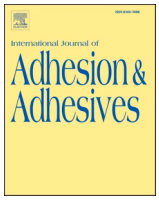

Ancient adhesives revisited: Unlocking potential for sustainable and renewable modern applications

A. Aleo [a,*], R. de Araujo Alves Lima [b,d], D. Molendijk - van den Hengst [c], R.W.A. Hendrikx [a], S. Teixeira de Freitas [b,d], G.H.J. Langejans [a,e], A.J. Böttger [a,c,**]

[a] Faculty of Mechanical Engineering – Materials Science and Engineering, Delft University of Technology, Mekelweg 2, Delft, 2628 CD, the Netherlands
[b] IDMEC, Instituto Superior Técnico – Av. Rovisco Pais 1, Lisbon, 1049-001, Portugal
[c] Centre of Expertise Safe & Resilient Society – New Materials and Applications, Avans University of Applied Sciences, Hogeschoollaan 1, Breda, 4818 CR, the Netherlands
[d] Faculty of Aerospace Engineering – Aerospace Structures and Materials, Delft University of Technology, Kluyverweg 1, Delft, 2629 HS, the Netherlands
[e] Palaeo-Research Institute, University of Johannesburg, 42 Bunting Rd, Johannesburg, 2092, South Africa

A B S T R A C T

Conventional petroleum-based adhesives present environmental challenges due to their toxicity, limited recyclability, and reliance on finite resources. Because ancient technology may serve as an inspiration for future solutions, the BiDebA (BioBased Debondable Adhesives) Interreg NWE project, systematically evaluated three archaeo-inspired bio-based adhesives –birch tar, rosin-beeswax blends and hide glue. The aim is to generate performance data relevant for future sustainable adhesive development. Natural additives used historically and in contemporary bio-based formulation research, including hematite and biochar, were incorporated to assess their influence on mechanical and thermal behaviour.

A multi-analytical approach combining single lap-shear testing, thermal and rheological characterisation, and structural analysis was performed. The adhesives exhibited average lap shear strengths between 1.5 and 3.5 MPa, consistent with other light-duty bio-based systems. Birch tar showed the broadest substrate compatibility, including effective bonding to plywood and carbon-fibre composites, while rosin-beeswax blends and hide glue demonstrated material-specific strengths and limitations. Among the fillers tested, hematite provided the most consistent enhancements, improving mechanical strength and thermal stability while lowering debonding temperatures, particularly in birch tar and rosin-based systems. This identifies hematite as a dual-function additive capable of tuning performance while maintaining reversibility, supporting the development of repairable and recyclable bio-based adhesive systems.

These findings highlight the value of archaeological adhesive technologies as informative material models rather than direct formulations. The dataset produced here also provides a scientific foundation for tailoring the mechanical and thermal behaviour of natural adhesives and supports ongoing efforts toward sustainable innovation in adhesive technology.

1. Introduction

Conventional adhesives are largely petroleum-derived, non-biodegradable, and may pose toxicity concerns, raising significant sustainability issues. Concurrently, the increasing use of adhesively bonded joints as an assembly method, owing to advantages over mechanical fastening such as reduced weight, minimised substrate damage, and more uniform stress distribution [1–3], has intensified end-of-life challenges. In particular, the recycling of bonded assemblies remains difficult. Bio-based adhesives offer a potential route towards improved sustainability, with advantages including renewability and biodegradability; however, their broader application is limited by inferior mechanical performance, restricted availability, and variability in properties [4,5]. In this paper we set out to help overcome some of these challenges by turning to the past for inspiration.

Prehistoric societies used natural adhesives –including plant resins, birch bark tar, and hide glue– sometimes enhanced with hematite, beeswax, or charcoal, for tool-making, waterproofing, and repair [6]. Previous research investigated their preparation and adhesive strength mainly to assess technological and cognitive complexity in early humans

* Corresponding author.
** Corresponding author. Faculty of Mechanical Engineering – Materials Science and Engineering, Delft University of Technology, Mekelweg 2, 2628 CD Delft, the Netherlands.
E-mail addresses: alealeo89@gmail.com (A. Aleo), rosemere.lima@tecnico.ulisboa.pt (R. de Araujo Alves Lima), d.molendijk@avans.nl (D. Molendijk - van den Hengst), R.W.A.Hendrikx@tudelft.nl (R.W.A. Hendrikx), sofia.teixeira.freitas@tecnico.ulisboa.pt (S. Teixeira de Freitas), G.Langejans@tudelft.nl (G.H.J. Langejans), A.J.Bottger@tudelft.nl (A.J. Böttger).

https://doi.org/10.1016/j.ijadhadh.2026.104387
Received 11 January 2026; Received in revised form 29 March 2026; Accepted 9 June 2026
Available online 12 June 2026

(e.g., Ref. [7–10]). However, up to date there is little systematic data that could inform modern technologies. Within the BiDebA Project (BioBased Debondable Adhesives, Interreg NWE) archaeologically and historically inspired bio-based adhesives and fillers were systematically tested to generate comparative performance data that can inform the development of modern, sustainable, and debondable adhesive technologies.

This study focuses on three archaeo-inspired bio-adhesives: (a) a rosin–beeswax blend, (b) birch bark tar, and (c) hide glue, applied to wood and carbon fibre-reinforced (CFRP) composites. These materials were selected because their constituent substances are among the earliest historically documented adhesive or binding materials (see SI). Additionally, they are manufactured from natural, renewable materials or from industrial by-products, thereby addressing waste management challenges and promoting a circular economy. Similarly, hematite (red ochre) and biochar, used here as a substitute for charcoal, were selected as additives for two main reasons. First, they are largely attested in prehistoric and historic adhesive formulations. Second, they provide functional benefits when incorporated into bio-based adhesives: (i) hematite improves strength and handling, while reducing tackiness [7,11], and (ii) biochar, a carbon-rich pyrolysis product, has been used ethnographically as a filler and is increasingly employed as a sustainable additive in polymers to improve chemical, structural, and thermal properties [6,12–14].

To evaluate these archaeo-inspired adhesives and fillers, comprehensive experimental analyses, including mechanical characterisation by means of single-lap-joint shear test (SLS), thermal analysis (differential scanning calorimetry - DSC, and thermogravimetric analysis - TGA), structural assessments (X-ray diffraction - XRD, and Fourier transform infrared spectroscopy - FTIR), and rheological measurements were conducted. These methodologies allowed the assessment of mechanical strength, thermal stability, debondability, and reusability of the studied adhesives, providing a robust dataset for understanding their fundamental properties and technological potential.

By linking ancient adhesive technologies with modern material analysis, this study establishes a scientific basis that can inform the future design and optimisation of sustainable bio-based adhesives.

2. Materials and methods

2.1. Adhesives

Three main archeo-adhesives were selected for that study: (a) rosin-beeswax blend, (b) birch tar, and (c) hide glue, which are described below. The archaeological background is given in the SI.

2.1.1. Rosin and beeswax

Rosin is the solid fraction of pine resin remaining after removal of volatile oils, primarily composed of abietic acid with a softening point of ~65–80 °C [15–17]. For this project, rosin (Cas. Nr.: 8050-09-7, EINECS-Nr: 232-475-7), in its solid form, was purchased from Verfmolen de Kat (The Netherlands). Its molecular composition is reported in Table S1, SI.

As pure rosin is brittle and prone to cracking, beeswax was added as a natural plasticiser. Beeswax has a partially crystalline structure with a melting range of 60–70 °C depending on origin [18]. For this project, 100% pure beeswax beads (CAS No. 8012-89-3, EINECS 232-383-7) were purchased from Kremer Pigmente (Germany). A rosin-beeswax blend (ratio 7:3) was used in this work.

2.1.2. Birch tar

Birch tar results from the thermal transformation of *Betula* sp. bark through pyrolysis under reduced-oxygen conditions, although experimental studies have shown that it can also form in more oxygenated settings [19]. The resulting material is a complex organic substance composed predominantly of insoluble, high-molecular-weight polymerised compounds with an asphaltene-like structure, whereas the solvent-soluble fraction constitutes only a minor proportion and is characterised by triterpenoids [20–22].

Birch tar lacks a sharp melting point. Therefore, it is typically hard and brittle below 30 °C, softens between 30 and 70 °C, and becomes semi-fluid to fluid above 80 °C [23]. Kiln-produced birch tar, in its solid form, was purchased from Asgaard-archery.nl (The Netherlands) and used in this study. Its molecular composition is reported in Table S1, SI.

2.1.3. Hide glue

Animal glues are derived from collagen hydrolysis, converting insoluble protein into soluble forms through thermal or chemical treatment [24,25]. Extraction is typically performed in hot water at 60–65 °C to maintain adhesive performance [6]. Protein-based glues provide good bonding strength but are moisture-sensitive and biodegradable. For this study, cowhide glue granules (280 Bloom), derived from cow hide collagen, were purchased from Verfmolen de Kat (The Netherlands). The dry mass consists predominantly of collagen protein (~85–89%), consistent with other commercial hide glue formulations.

2.2. Additives

2.2.1. Biochar

Biochar is a carbon-rich material produced by pyrolysis of biomass residues, including wood, agricultural by-products, and food waste [13,26]. A birch-spruce wood biochar made in Finland (Bio Char | Soil-Coco Upgrade - Eugardencenter.com) was used as a bio-based filler, serving as a sustainable analogue to prehistoric charcoal. The particle size ranges between ~0.05 mm and 2 mm.

2.2.2. Hematite (red ochre)

Hematite is an iron oxide pigment with archaeological evidence of human use dating back 250,000 years [27]. For this research, red ochre containing more than 80 wt% of iron oxide, and referred to as hematite, was purchased from Kremer Pigmente (Germany). The material used here contains >80 wt% Fe_2O_3, with SiO_2, Al_2O_3, CaO, and MgO as minor components (<10 wt% combined). The hematite average particle size is 1.25 ± 0.15 μm.

2.3. Substrates

To explore future applications of archeo-inspired adhesives and additives, two common substrate materials were selected for bonding.

2.3.1. Plywood

Multiplex hardwood panels of Meranti wood (~3.6 mm thick) were purchased from Praxis (The Netherlands). Technical specifications are listed in Table S2, SI.

2.3.2. Carbon fibre-reinforced (CFRP) composites

High-strength carbon fibre-reinforced composite (~2 mm thick, CFS-RI-1-0056) were obtained from Easy Composites (UK). The laminates feature quasi-isotropic fibre orientation [0/90/45/-45] in a high-performance epoxy matrix and XPREG XC130 Prepreg Carbon 3K. The visible surface has a high-gloss finish, while the reverse side has a flat, textured peel-ply finish. Mechanical properties are listed in Table S3, SI.

2.4. Adhesive preparation

Rosin and birch tar adhesives were heated on a hot plate (~100 °C) to achieve a viscous state. Rosin was mixed with beeswax (volume ratio 7:3 respectively) to reduce brittleness. Hide glue grains were dissolved in water (ratio 1:1.8 by weight) and gently heated in a water bath to avoid rapid temperature changes [28].

Hematite and biochar were added at 10 and 30 wt% to all adhesive formulations. The selected filler contents (10 wt% and 30 wt%) were

based on previous experimental studies on comparable bio-based adhesives [7,29]. Accordingly, 10 wt% was selected as a previously identified optimal reinforcement level, and 30 wt% as a higher-loading condition. Hematite powder was incorporated directly, while biochar, containing millimetric wood fragments, was first blended and sieved to collect the finer fraction (particle size ~0.05–0.7 mm).

2.5. Experimental methods

To assess the mechanical, thermal, and physicochemical properties of the selected archaeo-inspired adhesives, a series of experimental measurements was conducted (Table S4).

First, the base formulations were characterised using SLS testing, XRD, DSC, TGA, and rheology to determine debonding temperature. DSC, TGA, and rheology were not performed on hide glue due to its proteinaceous, non-thermoplastic nature, which renders thermal transitions and heat-induced debonding less relevant and incomparable to the other adhesives.

Next, the effects of hematite and biochar additives (10 and 30 wt%) on adhesive performance were evaluated using SLS tests. The best-performing mixtures were then analysed further to assess the impact of additives on thermal stability, physicochemical properties, and debondability using XRD, DSC, TGA, and rheology.

Finally, to investigate birch tar reusability (cf. [8]), the 30 wt% hematite mixture was subjected to controlled reheating cycles to simulate repeated reuse. One cycle represented minimal reuse, while five cycles were selected as a moderate repeated-use scenario to probe potential performance degradation. The adhesive was heated to 100–120 °C until fully melted, held for 2 min, cooled, and reheated. After one cycle, lap shear samples were prepared; the process was repeated four additional times. Total heating time was ~10 min for one cycle and ~20 min for five cycles. SLS, TGA, XRD, FTIR analyses were performed on the reheated samples.

2.5.1. Single-lap-joint shear (SLS) specimens

Single-lap-joints were produced in accordance with ISO 4587:2003 [30], using plywood and CFRP composites as substrates. Surface preparation is a key factor for adhesively bonded joint strength [31]; therefore, the following surface treatments were applied.

- Wood: the wood adherends were sanded with 180-grit sandpaper in a criss-cross pattern (±45°) and cleaned with 70% alcohol.
- CFRP composites: the rough peel-ply side was degreased with acetone and then exposed to UV-ozone surface treatment for 7 min using an in-house apparatus at the Faculty of Aerospace Engineering (TU Delft). The apparatus consists of three 30 W UV lamps with natural quartz sleeves (UV-Technik, Wümbach, Germany) emitting wavelengths of 184.9 nm and 253.7 nm. Such UV-Ozone treatment improves surface cleaning, eliminating any organic contamination as observed in Teixeira de Freitas et al. [32].

Substrates were pre-heated for 30 s on a hot plate to facilitate adhesive application and prevent rapid drying. Literature reports curing times of ~15 min for rosin and birch tar joints, and several hours for hide glue (e.g., Ref. [33,34]). To ensure complete curing in the absence of datasheet information, all samples in this study were cooled to room temperature (21–23 °C) and conditioned for at least 12 h before testing.

The standard [30] recommends an adhesive layer thickness of 0.2 mm; however, this parameter was difficult to control due to the absent of spacers or glass beads to regulate the bond line. On plywood substrates, additional variation arose from panel irregularities and surface sanding, which caused uneven bonded areas. Furthermore, the low-viscosity hide glue was rapidly absorbed into the porous wood, resulting in underestimated thickness measurements (average adhesive layer thickness 0.13 ± 0.08 mm). CFRP composites showed more reproducible results, owing to the lower internal variability of the composite sheets and the absence of surface sanding (average adhesive layer thickness 0.32 ± 0.23 mm). Overall, samples containing additives exhibited greater adhesive layer thicknesses. In particular, biochar fragments increased thickness variability and occasionally disrupted joint alignment (see Table S5–S6).

SLS tests were performed using a Zwick-Roell Z010 tensile bench with a 100 kN load cell at 1.3 mm/min and a 10 N preload. Each adhesive mixture was tested using n = 10 independent specimens for plywood substrates and n = 5 for CFRP composites. These sample sizes were selected to ensure statistical robustness while accounting for material availability and variability.

To assess statistical significance of shear strength differences between adhesive mixtures, normality was evaluated using the Shapiro-Wilk test. Groups with normally distributed data were analysed using Student's *t*-test, while non-normal data were analysed using the Mann-Whitney *U* test. Analyses were performed in PAST v4.03.

2.5.2. Materials characterisation methods

XRD was performed using a Bruker D8 Discover diffractometer equipped with an Eiger-2 500k 2D-detector. An Incoatec 1 μS microfocus tube with Cu Kα radiation was employed, operating at 50 kV and 1000 μA. A scatter screen and a UBC collimator of 0.5 mm (for birch tar and hide glue) and 1 mm (for beeswax, rosin, and mixtures) were used. A coupled θ–2θ scan was carried out over the angular range of 5 to 60 °2θ, with a step size of 0.02 °2θ and a counting time of 1 s per step (for birch tar and hide glue) and 2 s per step (for beeswax, rosin, and mixtures). The acquired diffraction data were processed and analysed using Bruker DiffracSuite.EVA software 7.3. For identification, the ICDD PDF5 and COD databases were used. The coloured sticks in the graphs give the peak positions and intensities of the possibly present crystalline phases based on this identification. The degree of crystallinity was determined by dividing the integrated intensity of the crystalline diffraction peaks by the total integrated intensity (the sum of the crystalline and amorphous contribution) between 5 and 60 °2θ. This approach provides a semi-quantitative measure of the relative crystalline order within the samples.

DSC of TA Instruments (Q200) was used to determine the melting temperature (T_m) of the materials using aluminium cups as sample holders. The DSC analysis was conducted over the temperature range of −20 °C and 100 °C, with a multi-part sequence consisting of cooling to the start point, heating until 100 °C, cooling until −20 °C, reheating until 100 °C, with the heating and cooling rates set at 20 °C/min. The T_m was determined using the first heating cycle by measuring the peak in the first derivative of the heat flow vs. temperature curve. Integration of the curve at T_m resulted in the melting enthalpy (ΔH_m).

TGA was conducted using a TA Instruments (Q50). Samples were heated to 600 °C with a heating rate of 20 °C/min under nitrogen atmosphere, whilst monitoring weight change. The degradation temperature ($T_{50\%}$) was determined by measuring the peak in the first derivative of the weight change vs. temperature curve. Additionally, the exact mass of added hematite was determined by analysing the mass of the residue which remained in the sample at 600 °C.

Rheology measurements were conducted using a rheometer by TA Instruments (HR20) in a 25 mm parallel plate setup. Solid samples were added to the plate and molten by heating to 100 °C with a heating rate of 20 °C/min and with a constant axial compression force of 5 N to form a measurable sample in a 1000 μm gap. The samples were passively cooled to room temperature before heating to 120 °C with a heating rate of 10 °C/min and a constant axial tension force of 1 N, while continuously monitoring the gap change. The debonding temperature was determined by analysing the onset point in the gap vs. temperature curve.

FTIR analysis was performed on a Bruker Alpha II system equipped with a platinum diamond ATR module (#DA971F62D), collecting spectra over a wavenumber range of 400–4000 cm^{-1}. Each sample spectrum was acquired as the average of 24 scans at a nominal resolution of 4 cm^{-1}. A background spectrum, also recorded as the average of

24 scans, was performed before each measurement to ensure a reliable baseline correction and to compensate for atmospheric CO_2/H_2O.

Unless stated otherwise, material characterisation techniques (XRD, DSC, TGA, rheology, and FTIR) were performed on one representative specimen (n = 1) per adhesive formulation of interest. These measurements were intended to provide comparative, semi-quantitative insights into material behaviour and compositional differences between mixtures.

3. Results

3.1. Material properties of pure adhesive materials

3.1.1. Single-lap-joint shear (SLS) test

Fig. 1 (a) and (b) show the representative load-displacement curves of the SLS joints bonded with the studied adhesives. As shown, the plywood specimens exhibited overlapping curves with nearly identical stiffness, regardless of the adhesive type used. However, different maximum force values were observed. The highest value was obtained by the plywood joints bonded with hide glue (around 800 N), followed by rosin-beeswax (600 N) and birch tar (400 N). A diverse behaviour was instead observed in the CFRP composites. The hide glue exhibited the lowest maximum force (100 N) and a higher displacement, without brittle failure, while birch tar displayed the highest maximum force (above 800 N). The rosin-beeswax blend showed a similar maximum force value to those of the plywood joints.

Fig. 1 (c and d) presents the shear strength of the plywood and CFRP composite joints, respectively, while Fig. 2 illustrates representative fracture surfaces corresponding to the failure modes discussed in the text.

The following main outcomes can be taken.

3.1.1.1. Plywood. Pure hide glue was the best-performing adhesive for plywood (Fig. 1c), reaching an average maximum lap shear strength of 3.56 ± 0.49 MPa (Table S7). For all the samples, the failure was of the substrate, either stock-break or fibre-tear (Fig. 1e, Fig. S1), indicating that the adhesive bond strength exceeded that of the substrate. The rosin-beeswax (7:3) blend had an average maximum lap shear strength of 1.56 ± 0.55 MPa (Table S7). The failure types observed are cohesive or thin cohesive (Fig. 1e, Fig. S2), meaning that the failure occurred at the intramolecular bond within the adhesive. All rosin-beeswax (7:3) samples exhibited 100% brittle fracture, characterised by a sudden failure with minimal plastic deformation (Fig. S4). Birch tar had an average maximum lap shear strength of 1.24 ± 0.45 MPa (Table S7), with failure types also classified as cohesive or thin cohesive (Fig. 1e, Fig. S3). Fracture analysis revealed a mixed mode in the birch tar samples: approximately 70% brittle and 30% ductile (Fig. S7). This heterogeneous behaviour is likely attributable to substrate thickness variability causing non-uniform adhesive thickness.

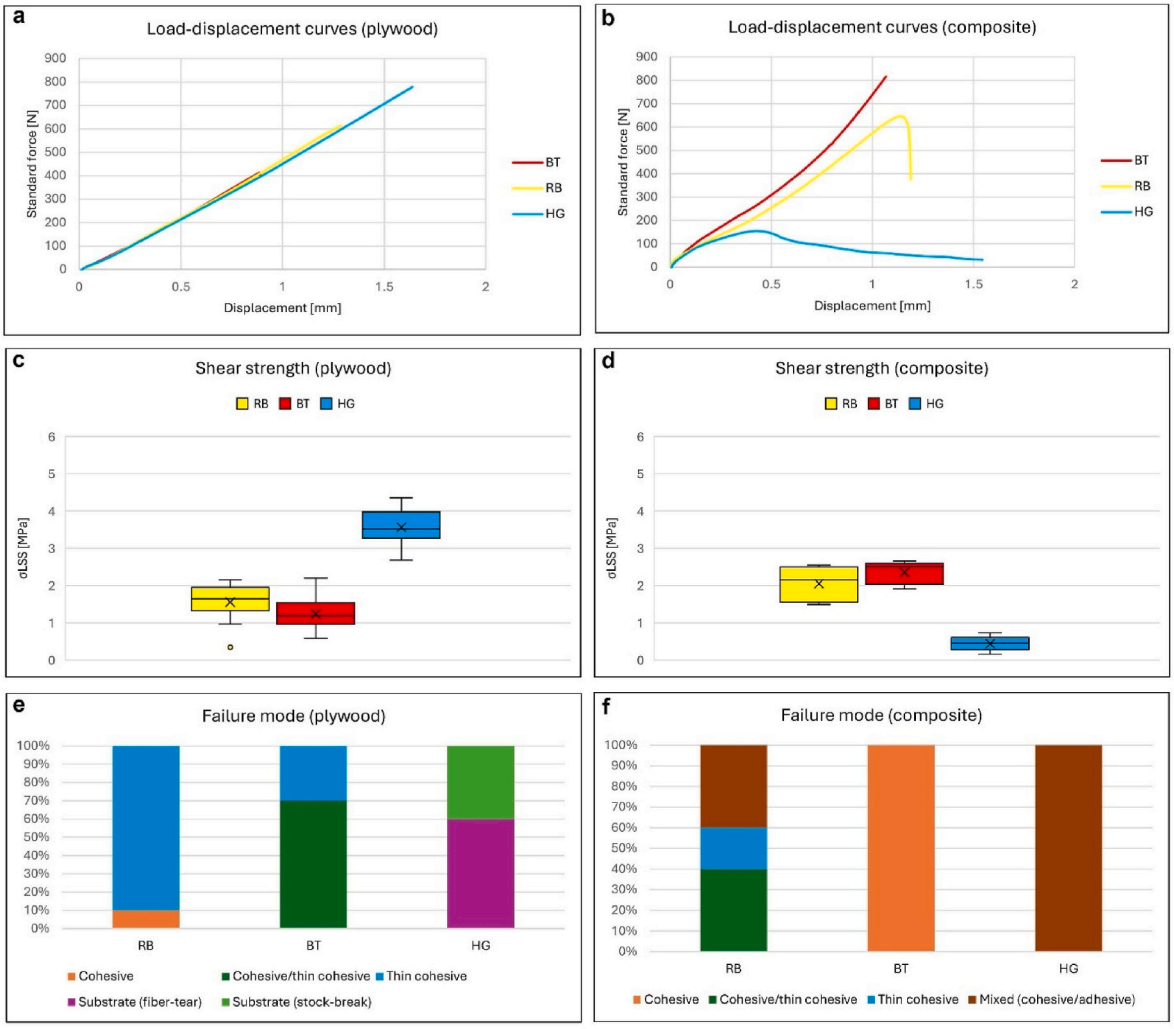

Fig. 1. Comparison of rosin-beeswax (7:3), birch tar, and hide glue in plywood (left) and CFRP composites (right). a-b) representative load-displacement curves illustrating mechanical behaviour under stress; c-d) shear strength of adhesives; e-f) failure modes.

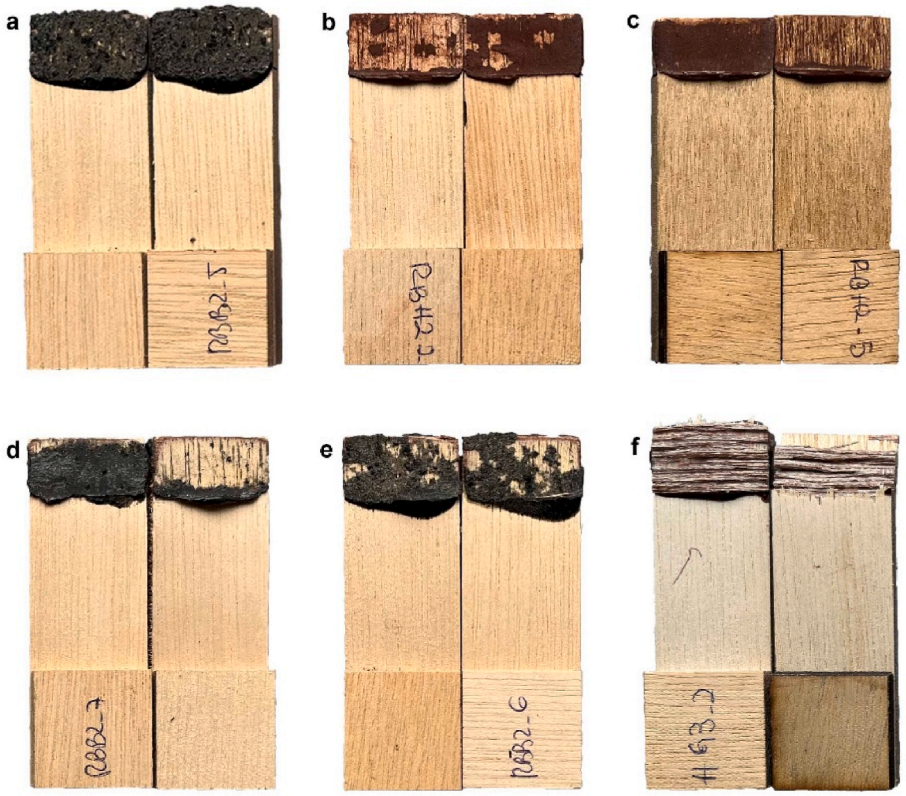

Fig. 2. Representative fracture surfaces observed after testing. a) cohesive failure; b) cohesive/thin cohesive failure; c) thin cohesive failure; d) cohesive/adhesive failure; e) mixed-mode cohesive and adhesive failure; f) substrate failure.

3.1.1.2. Carbon fibre-reinforced (CFRP) composites. For CFRP composites, birch tar was the best-performing adhesive (Fig. 1d) reaching an average maximum lap shear strength of 2.35 ± 0.31 MPa (Table S7). Birch tar bonded well with the substrate, and in all the samples, the failure was cohesive (Fig. 1f, Fig. S3). Birch tar samples exhibited 100% brittle fracture, characterised by a sudden failure with little to no plastic deformation (Fig. S7). In contrast to the results obtained with plywood joints, the performance of hide glue on CFRP composites was poor (Fig. 1d), with an average maximum lap shear strength of 0.44 ± 0.20 MPa (Table S7). Hide glue did not bond well with the substrate, and in all samples, the failure mode was mixed adhesive and cohesive (Fig. 1f, Fig. S1). The fracture type was 100% ductile, with load-strain curves showing gradual failure progression (Fig. S9). The rosin-beeswax (7:3) blend performed intermediately between birch tar and hide glue, reaching an average maximum lap shear strength of 2.05 ± 0.48 MPa (Table S7). Observed failure modes were cohesive/thin cohesive or mixed (cohesive and adhesive) (Fig. 1f, Fig. S2), and the fracture type was predominantly ductile (Fig. S5).

3.1.2. Structural characterisation: X-ray diffraction (XRD)

Fig. 3 presents the XRD patterns of the analysed archaeo-inspired adhesives, revealing distinct differences in their degree of crystallinity. The diffraction pattern of pure rosin shows a broad diffuse peak of an amorphous phase in the measured 2θ-range (10-70° 2θ) with maximus at around 2θ ≈ 20° and 2θ ≈ 45° (Fig. 3a) as typically observed in amorphous rosins [18]. Two small diffraction peaks matching reference patterns attributed to long-chain aliphatic compounds such as Carnauba wax (ICDD card no 00-072-1406) are also visible between 20 and 25 °2θ.

The diffraction pattern of beeswax displays sharp and pronounced diffraction peaks (Fig. 3b) specific for the molecular structure of myricyl-palmitate, $C_{15}H_{31}CO\text{-}O\text{-}C_{30}H_{61}$ (ICDD card no 00-063-1511), a typical abundant ester present in beeswax [18,35].

When rosin and beeswax are combined, the diffraction pattern of the rosin-beeswax (7:3) blend remains dominated by the diffraction peaks of crystalline myricyl-palmitate (Fig. 3c), indicating that the adhesive retains crystallinity arising from wax crystalline domains dispersed within an amorphous rosin matrix. The rosin-beeswax (7:3) blend exhibits a high relative crystallinity of ca. 80%. Such high crystallinity is expected to reduce wettability and ductility by limiting molecular mobility and interfacial flow.

The pattern of birch tar shows evidence of at least two crystalline phases, one observed by two strong peaks around 2θ ≈ 22 and 25° 2θ associated with long-chain aliphatic compounds matching reference patterns such as Carnauba wax (ICDD card no 00-072-1406) and one of plant-based triterpenoids Friedelin (D:A-Friedooleanan-3-on; $C_{30}H_{50}O$; ICDD card no 02-066-6893) (Table 1), which are consistent with the known composition of birch bark tar [36]. These sharp reflections, superimposed on a broad underlying hump between 10° and 35° 2θ, indicate the coexistence of crystalline and amorphous components. A substantially lower relative crystallinity (~16%) than for the rosin-beeswax blend is found. This structural nature is consistent with a softer and more ductile material that likely exhibit improved wetting behaviour. Such structural characteristics may explain the superior adhesion of birch tar compared to the rosin-beeswax blend, particularly on CFRP composites, where the more flexible and amorphous nature of birch tar facilitates better interfacial adaptation to smooth, low-energy surfaces.

Hide glue, by contrast, is characterised by an almost fully amorphous structure (relative crystallinity is <1%). Its XRD pattern shows a broad hump in the 2θ range from 10 to 30°, maximizing at around 2θ ≈ 20° typical of amorphous materials (Fig. 3g). In the XRD pattern of hide glue the bassanite ($2CaSO_4{\cdot}H_2O$; ICDD card no 00-002-0667) is likely due to contamination from manufacturing. In this case, the amorphous polar hydrogen-bonded structure allows excellent adhesion to polar porous substrates, such as wood. Conversely, the little chemical compatibility and poor wetting on the non-polar composite surface is responsible for

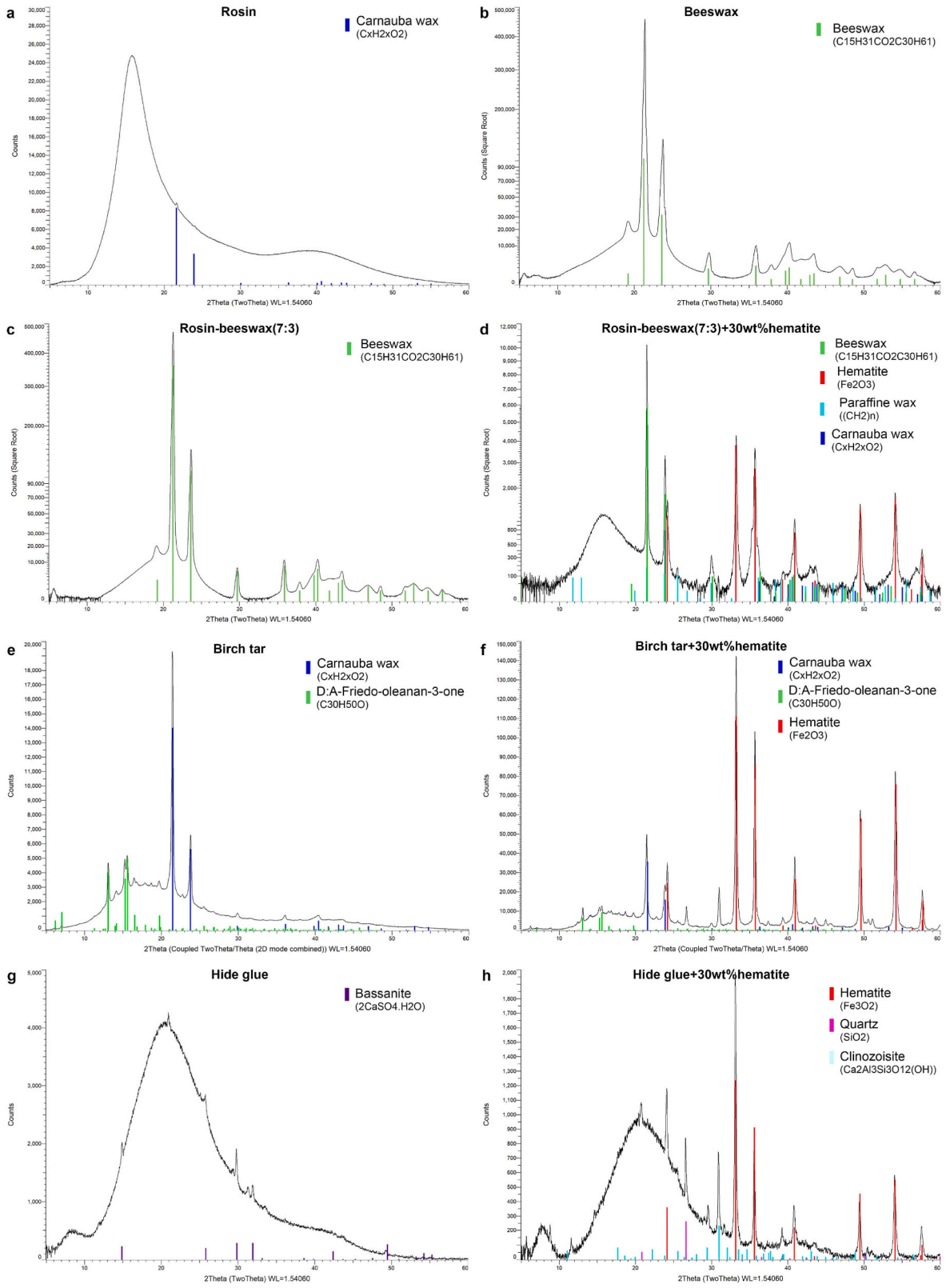

Fig. 3. XRD patterns of archaeo-inspired adhesives with and without hematite particles. Note the use of square root of counts for clarity in figs. b, c, and d.

the poor adhesive performance.

It should be noted that phase identification in XRD is based on database matching of diffraction patterns and, for complex organic mixtures such as natural resins and tars, should be interpreted with caution. In such systems, peak assignments may reflect structural similarities between compound classes (e.g., long-chain aliphatics or terpenoid derivatives) rather than the definitive presence of a specific reference compound.

Table 1
Summary of results of XRD, DSC, TGA, and rheology analyses of archaeo-inspired adhesives samples with and without additives hematite. **This enthalpy value is corrected for the weight of the red ochre and rosin.

Adhesive type	XRD	DSC		TGA		Rheology	FTIR
	Identification	T melt (°C)	ΔHm (J/g)	T50% (°C)	Residue (%)	Tdebonding (°C)	Peak location
Rosin	Amorphous Carnauba wax	55 (Tg)	N.A.	288	0	94.5	N.A.
Beeswax	Beeswax (myricyl-palmitate)	65	177	372	0	N.A.	N.A.
Rosin-beeswax (7:3)	Beeswax (myricyl-palmitate)	64	138 171**	399	0	58	N.A.
Rosin-beeswax (7:3)+ 30 wt%hematite	Carnauba wax Hematite Fe_2O_3 Paraffine wax	55	41 54.5**	351	24.5	57	N.A.
Birch tar	Carnauba wax Friedelin	65.5	51	343	5.2	99	2917, 2849, 1735, 1713, 1604, 1515, 1463, 1384, 1358, 1270, 1171, 1109, 1034, 880, 720 cm^{-1}
Birch tar reheated x1	Carnauba wax Friedelin	N.A.	N.A.	375	19	N.A.	Same as birch tar
Birch tar reheated x5	Carnauba wax Friedelin	N.A.	N.A.	391	25	N.A.	Same as birch tar
Birch tar+ 30 wt% hematite	Carnauba wax Hematite Fe_2O_3 Friedelin	65	42.5 64.9**	381	36	69	2916, 2848, 1733, 1712, 1604, 1513, 1462, 1384, 1358, 1270, 1168, 1109, 1031, 880, 720, 527, 444 cm^{-1}
Birch tar+ 30 wt% hematite reheated x1	Carnauba wax Friedelin	N.A.	N.A.	372	53	N.A.	Same as birch tar+30 wt%hematite
Birch tar+ 30 wt% hematite reheated x5	Carnauba wax Friedelin	N.A.	N.A.	367	54	N.A.	Same as birch tar+30 wt%hematite
Hide glue	Amorphous Bassanite	N.A.	N.A.	N.A.	N.A.	N.A.	N.A.
Hide glue+ 30 wt% hematite	Amorphous Hematite Fe_2O_3 Quartz SiO_2 Clinozoisite	N.A.	N.A.	N.A.	N.A.	N.A.	N.A.

3.1.3. Thermal properties: thermogravimetric analysis (TGA) and differential scanning calorimetry (DSC)

Fig. 4 presents the TGA curves of the investigated adhesive components and blends. The thermal decomposition of rosin starts around 200 °C and ends just after 350 °C, leaving nearly 0% residue (Table 1). Its degradation curve shows a gradual slope above 250 °C, followed by a sharp drop between 275 and 350 °C, indicating rapid volatilization (Fig. 4a). Beeswax begins to decompose at a slightly higher temperature, with onset near 300 °C, and completes decomposition just below 400 °C, also leaving negligible residue (Table 1). The rosin-beeswax (7:3) blend exhibits a slightly broader degradation window, between approximately 270 °C and 425 °C (Table 1). In contrast, the thermal decomposition of pure birch tar starts around 275 °C and extends up to nearly 500 °C, with a broad, gradual degradation curve (Fig. 4b) and a residual mass of ~5% (Table 1). The TGA results are consistent with Kozowyk & Poulis [8] in terms of overall trends and temperature ranges.

Fig. 5 displays the DSC thermograms in the range from −20 °C to 100 °C for rosin blends and birch tar blends. The curve of beeswax features a broad and pronounced endothermic peak centred around ~65 °C. The thermogram and melting enthalpy comply with that generally observed for beeswax [18]. In contrast, rosin displays no melting in the thermograms (cf. Gillard et al., 2011), confirming its amorphous structure accompanied by a glass-rubber transition (T_g) at ~55 °C. The mixture of rosin-beeswax (7:3) produces an intermediate DSC curve, less pronounced than that of pure beeswax (Fig. 5). This broadening indicates reduced crystalline order compared to pure beeswax, consistent with the XRD results showing a mixed structure. The apparent reduction of the melting enthalpy (ΔH_m) is an effect of the addition of rosin to the beeswax, which does not undergo the same phase transition. Subtracting the mass of rosin from the total sample mass results in same melting enthalpy value as for the beeswax (see Table 1). Therefore, the addition of rosin does not disrupt the crystallinity of beeswax.

The DSC curve of birch tar shows a broad melting range consistent with its complex composition and largely amorphous nature and a moderate melting enthalpy ΔH_m (Table 1). Several endothermic reactions occur with overlapping transitions (Fig. 5), likely attributable to the melting of various crystalline domains (or unidentified phases) present in the mixture. DSC thermograms of birch tar adhesives are not available in the literature therefore a direct comparison cannot be made.

To summarise, compared to birch tar, rosin-based blends degrade at lower temperatures and more completely, reflecting a more simple and more volatile chemical structure. Birch tar exhibits better thermal resistance and retains more mass upon reheating possibly due to the formation of new links. Based on the onset of major thermal degradation (250–300 °C), these adhesives are thermally stable up to approximately 150–200 °C for practical use. Pure rosin-based adhesives would be suitable below ~100–120 °C while rosin-beeswax blends and birch tar to approximately 150–180 °C. Service temperature limits were estimated from the TGA degradation onset using a 100 °C safety margin in accordance with ASTM E2550 [37].

3.1.4. Rheology and debonding temperatures

Pure rosin has a debonding temperature of 94.5 °C, which is higher than the glass-rubber transition temperature of rosin at ~55 °C (Table 1). When beeswax is added to rosin, the resulting debonding temperature of the rosin-beeswax (7:3) blend is about 58 °C (Table 1). Pure birch tar has a debonding temperature of about 99 °C, which is higher than the birch tar melting temperature of 65.5 °C (Table 1).

3.2. The effect of additives on adhesive's material properties

3.2.1. Single-lap-joint shear (SLS) test

Fig. 6 shows representative load-displacement curves of the SLS joints bonded with the studied adhesives, modified with hematite and biochar.

The rosin-beeswax (Fig. 6a and b) and birch tar (Fig. 6c and d) formulations exhibit generally comparable stiffness across all variants for

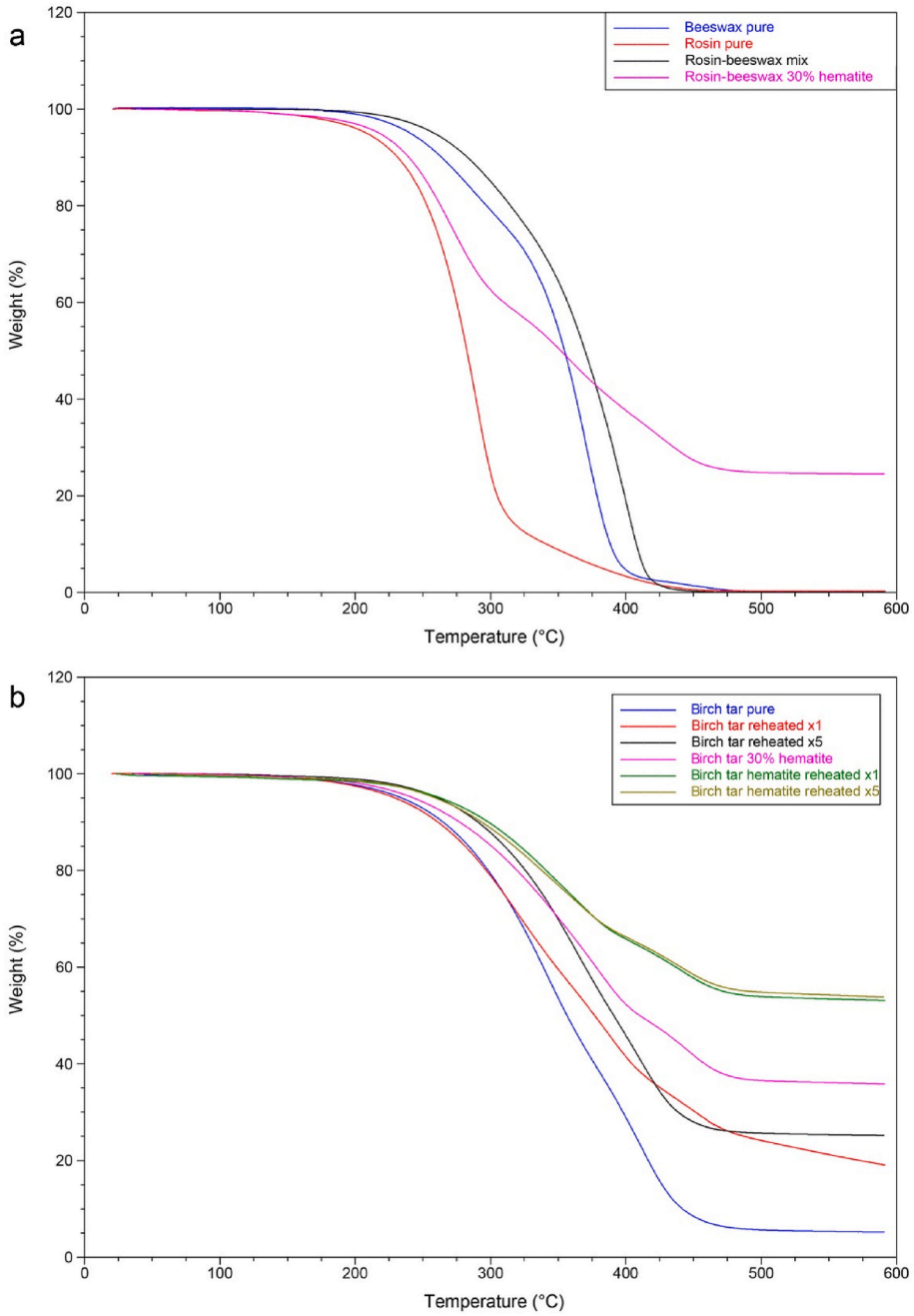

Fig. 4. TGA curves displaying the weight loss (%) of rosin blends (a) and birch tar blends (b) during heating from 0 °C to 600 °C in nitrogen atmosphere.

both plywood and CFRP composites, with only minor differences in maximum force values. Overall, the addition of hematite increased the maximum load capacity, particularly in the birch tar formulations, whereas the addition of biochar –especially at higher concentrations– reduced the maximum force while increasing displacement.

In contrast, significant differences were observed for hide glue (Fig. 6e and f) depending on both the additives and the substrate. For plywood specimens, all formulations except the one containing 30 wt% biochar failed at the substrate. The 30 wt% biochar formulation markedly reduced both stiffness and maximum load, reaching higher values of displacement, indicative of progressive rather than brittle failure. In composite joints, hide glue displayed the lowest loads among the adhesives tested. The unmodified hide glue formulation reached maximum forces of 150–200 N, followed by a gradual decline without brittle fracture. All modified systems showed similar trends, but the addition of hematite to hide glue (10 wt% or 30 wt%) significantly increased the maximum load compared to the base adhesive. The 30 wt% biochar formulation performed poorly, showing very low stiffness and extended displacement after the peak, consistent with progressive, ductile-like failure.

Figs. 7 and 8 present the joint's shear strength of the plywood and CFRP composites, respectively, and the following main outcomes can be taken.

3.2.1.1. Plywood. Table S8 summarises the results of lap shear tests using plywood adherends, evaluating rosin-beeswax (7:3) blend, birch tar, and hide glue adhesives modified with 10 wt% and 30 wt% hematite and biochar.In the rosin-beeswax (7:3) blend, the addition of 10 wt% and 30 wt% hematite resulted in reductions in the average lap shear strength of approximately 9% (from 1.56 ± 0.55 MPa to

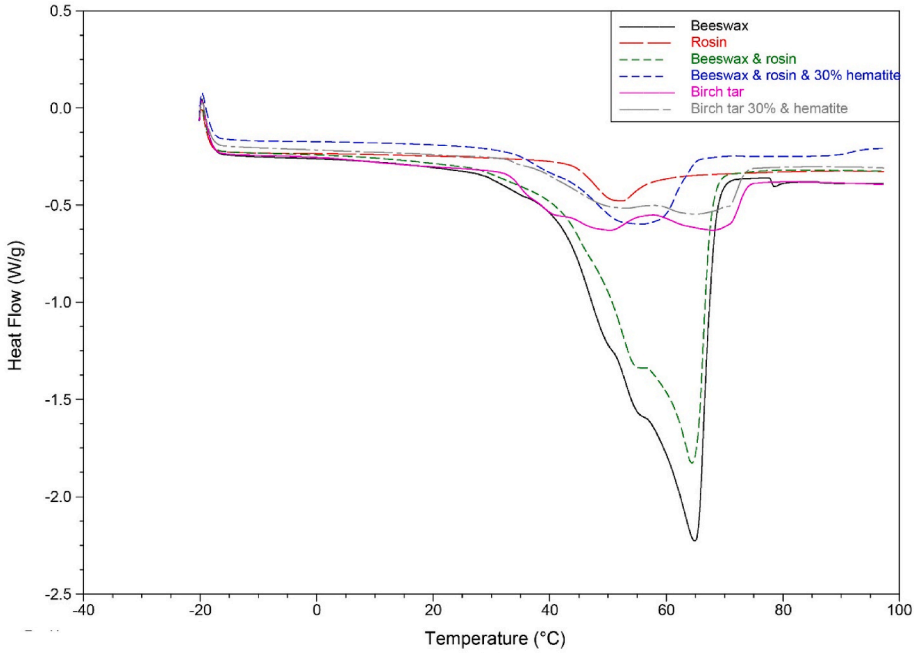

Fig. 5. DSC thermograms in the range from −20 °C to 100 °C for rosin blends and birch tar blends.

1.42 ± 0.32 MPa) and 30% (to 1.08 ± 0.37 MPa), respectively (Fig. 7a). Biochar addition also reduced the average lap shear strength: 10 wt% caused a significant ~52% decrease (to 0.74 ± 0.55 MPa; *t*-test, $p < 0.05$), while 30 wt% led to a minor ~6% reduction (to 1.46 ± 0.34 MPa) (Fig. 7c). Failure in these samples was predominantly cohesive or thin cohesive. Some initially appeared to show near-adhesive failure; however, closer inspection of the fracture surfaces revealed adhesive residues within wood micro-cracks and pores. These were therefore classified as thin cohesive/adhesive failures (Fig. 7b–d; Fig. S2). Mixtures of rosin-beeswax (7:3) with 30 wt% hematite and 10 wt% biochar exhibited fully brittle fracture (Fig. S4). In contrast, samples containing 10 wt% hematite or 30 wt% biochar displayed a mixed fracture mode: approximately 60% brittle and 40% ductile (Fig. S4). This heterogeneous behaviour may result from a combination of factors, including substrate and adhesive variability, non-uniform surface preparation, uneven adhesive layer thickness, or inhomogeneous filler dispersion.

For birch tar, the addition of hematite resulted in a statistically significant increase in the average lap shear strength: ~28% with 10 wt% (from 1.24 ± 0.45 MPa to 1.59 ± 0.24 MPa; *t*-test, $p < 0.05$) and ~64% with 30 wt% (to 2.03 ± 0.49 MPa; *t*-test, $p < 0.05$). Similarly, 10 wt% biochar significantly improved the average lap shear strength by ~60% (to 1.99 ± 0.40 MPa; *t*-test, $p < 0.05$), whereas 30 wt% biochar had no notable effect (Fig. 7c). Across all birch tar-based samples, failures were primarily cohesive or thin cohesive (Fig. 7b–d; Fig. S3). The addition of hematite and 10 wt% biochar increased adhesive stiffness and peak load (Fig. S6). In contrast, 30 wt% biochar led to a significant reduction in peak load and a shift toward more ductile fracture behaviour (Fig. S6).

The addition of hematite (both concentrations) and 10 wt% biochar did not negatively affect the average lap shear strength of hide glue (Fig. 7a–c). Variations in lap shear strength appeared to correlate with differences in the fracture patterns of the wood adherends. In most cases, failure occurred within the wooden substrate, either as fibre-tear or stock-break (Fig. 7b–d; Fig. S1). However, incorporation of 30 wt% biochar significantly reduced the average lap shear strength of hide glue from 3.56 ± 0.49 MPa to 1.30 ± 0.28 MPa (*t*-test, $p < 0.001$), with failure modes shifting toward predominantly cohesive or adhesive failure and minimal substrate involvement (Fig. 7d, Fig. S1). Load-strain curves for hide glue containing 30 wt% biochar showed a significantly reduced peak load and a ductile response, characterised by smoother curves and progressive failure (Fig. S8).

3.2.1.2. Carbon fibre-reinforced (CFRP) composites. Table S9 summarises the results of lap shear tests using CFRP composites, evaluating rosin-beeswax (7:3) blend, birch tar, and hide glue adhesives modified with 10 wt% and 30 wt% hematite and biochar.In the rosin-beeswax (7:3) blend, the addition of 10 wt% hematite resulted in a ~5% decrease in the average lap shear strength (from 2.05 ± 0.48 MPa to 1.95 ± 0.17 MPa), whereas 30 wt% hematite increased it by ~15% (to 2.35 ± 0.31 MPa) (Fig. 8a). The addition of 10 wt% and 30 wt% biochar decreased the average lap shear strength by ~15% (to 1.74 ± 0.33 MPa) and ~45% (to 1.12 ± 0.07 MPa; *t*-test, $p < 0.01$), respectively (Fig. 8c). Across all samples, the observed failure modes were cohesive or thin cohesive (Fig. 8b–d; Fig. S2). The addition of both hematite and biochar increased adhesive stiffness, resulting in a shift toward more brittle fracture, particularly at higher additive concentrations. Higher concentrations of hematite led to increased peak load, while biochar additions caused a reduction in peak load (Fig. S5).

For birch tar, the addition of 10 wt% and 30 wt% hematite increased the average lap shear strength by ~2% (from 2.35 ± 0.31 MPa to 2.40 ± 0.37 MPa) and ~27% (to 2.98 ± 0.44 MPa; *t*-test, $p < 0.05$), respectively (Fig. 8a). Similarly, adding 10 wt% biochar increased the average lap shear strength by ~2% (to 2.39 ± 0.07 MPa), while 30 wt% biochar significantly reduced it by ~40% (to 1.42 ± 0.42 MPa; *t*-test, $p < 0.01$). All samples exhibited cohesive failure modes (Fig. 8b–d; Fig. S3). Tar samples with 10 wt% hematite failed in a fully brittle manner, characterised by sharp load drops and negligible post-yield deformation (Fig. S7). In contrast, samples containing 30 wt% hematite or biochar displayed a more ductile response, with smoother load-strain curves and progressive failure (Fig. S7).

For hide glue, the addition of 10 wt% and 30 wt% hematite significantly increased the average lap shear strength by ~125% (from 0.44 ± 0.20 MPa to 0.99 ± 0.13 MPa; *t*-test, $p < 0.01$) and ~164% (to 1.16 ± 0.46 MPa; *t*-test, $p < 0.05$), respectively (Fig. 8a). In contrast, adding 10 wt% and 30 wt% biochar significantly reduced the average lap shear strength by ~54% (to 0.20 ± 0.12 MPa; *t*-test, $p < 0.05$) and ~75% (to 0.11 ± 0.06 MPa; Mann-Whitney *U* test, $p < 0.05$), respectively (Fig. 8c). All hide glue samples exhibited mixed-mode cohesive

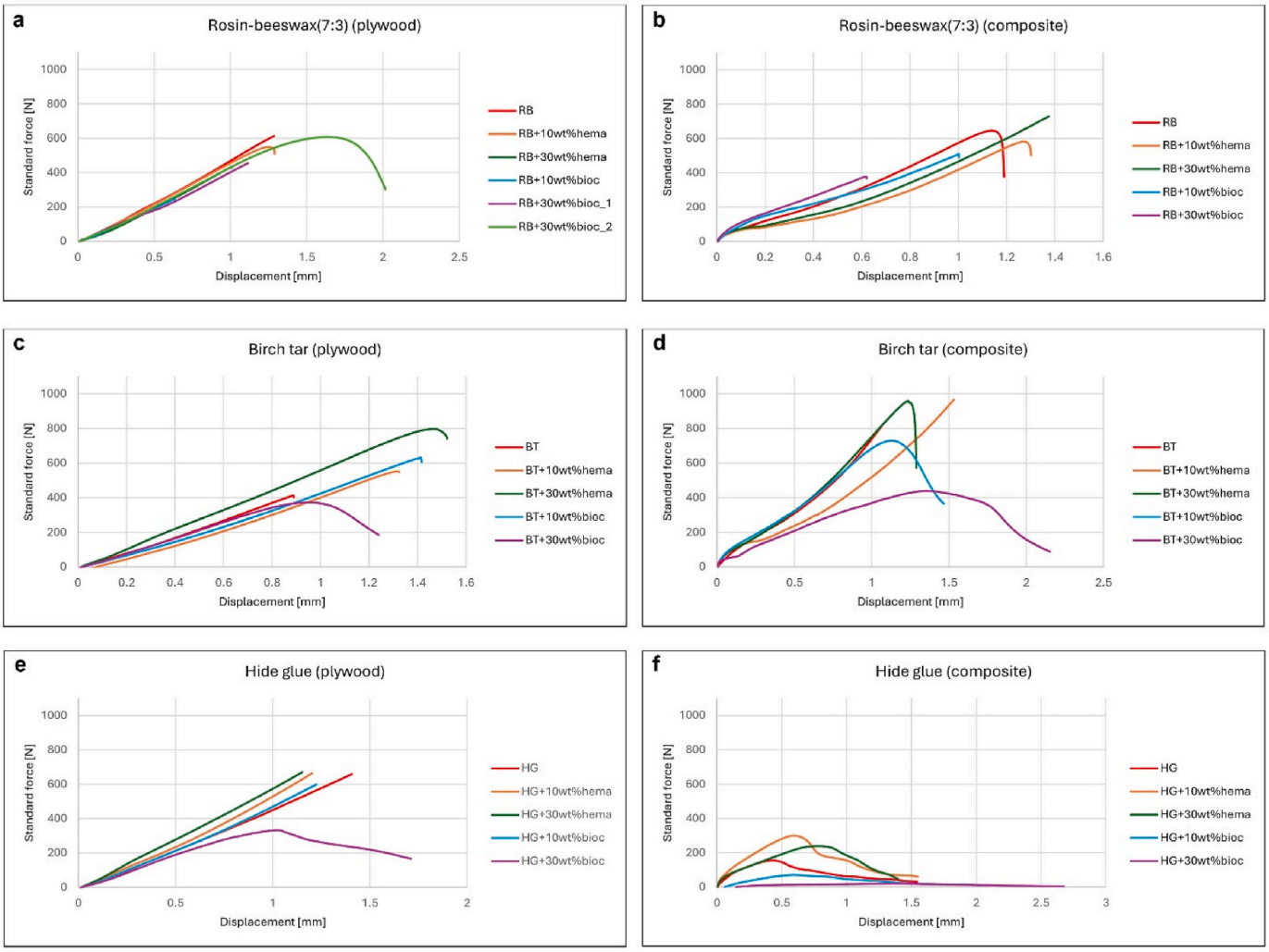

Fig. 6. Comparison of a-b) rosin-beeswax (7:3), c-d) birch tar e-f) hide glue representative load-displacement curves illustrating mechanical behaviour under stress in plywood (left) and CFRP composites (right). For the rosin-beeswax+30 wt%biochar two curves were selected to account for the mixed fracture behaviour observed in the samples.

and adhesive failure (Fig. 8b–d; Fig. S1) and failed in a ductile manner. Samples containing hematite showed a significant increase in peak load, whereas those with biochar showed a marked decrease (Fig. S9).

To summarise, birch tar was the overall best-performing adhesive, with the formulation containing 30 wt% hematite emerging as the optimally performing modified adhesive for both plywood and composite substrates. Among the rosin-beeswax (7:3) blends, the formulation with 30 wt% hematite showed the best performance on CFRP composites. Hide glue proved highly effective for wood bonding but exhibited limited applicability on the composite substrates, even when modified with additives. Overall, the addition of biochar generally reduced the average lap shear strength of the tested adhesives. Based on these considerations, only formulations of birch tar and the rosin-beeswax (7:3) blend containing hematite were selected for further analysis, focusing on the effects of hematite on the thermal stability, debondability, and physicochemical structure of the adhesives.

Additionally, due to its superior performance among the birch tar blends, the formulation containing 30 wt% hematite was selected to evaluate the reusability of birch tar adhesives, as suggested in the literature (cf. [8]). Our results were compared with those from the reheated birch tar sample without hematite filler and with published data [10,29].

3.2.2. *Structural characterisation: X-ray diffraction (XRD)*

All the diffraction patterns after the addition of hematite show the characteristics of its rhombohedral crystal structure (ICDD card no 01-089-8103). The patterns of the mixtures of rosin-beeswax (7:3), tar with hematite do not show any changes in peak position nor appearance of new peaks suggesting that the formation of new compounds or reaction between hematite and the organic adhesives is not pronounced if any (Fig. 3d–f). An exception may be the Clinozoisite ($Ca_2Al_3Si_3O_{12}(OH)$; ICDD card no 00-013-0563) observed in the XRD pattern of hide glue with 30 wt% hematite (Fig. 3h). Its occurrence could be the results of reaction of the bassanite with the Al- and Si- oxides present in the red ochre (hematite) additive during glue preparation.

Overall, the XRD patterns of the hematite-filled rosin-beeswax, birch tar, and hide glue adhesives reveal distinct crystalline domains associated with the dispersion of mineral particles within the organic matrices. As a result of hematite incorporation, the adhesives become less amorphous, and composite structures with multiple crystalline phases are introduced. This increased crystallinity can enhance hardness and internal cohesion but may also increase brittleness and reduce film thickness.

3.2.3. *Thermal properties: thermogravimetric analysis (TGA) and differential scanning calorimetry (DSC)*

Across both adhesive groups, the addition of hematite consistently

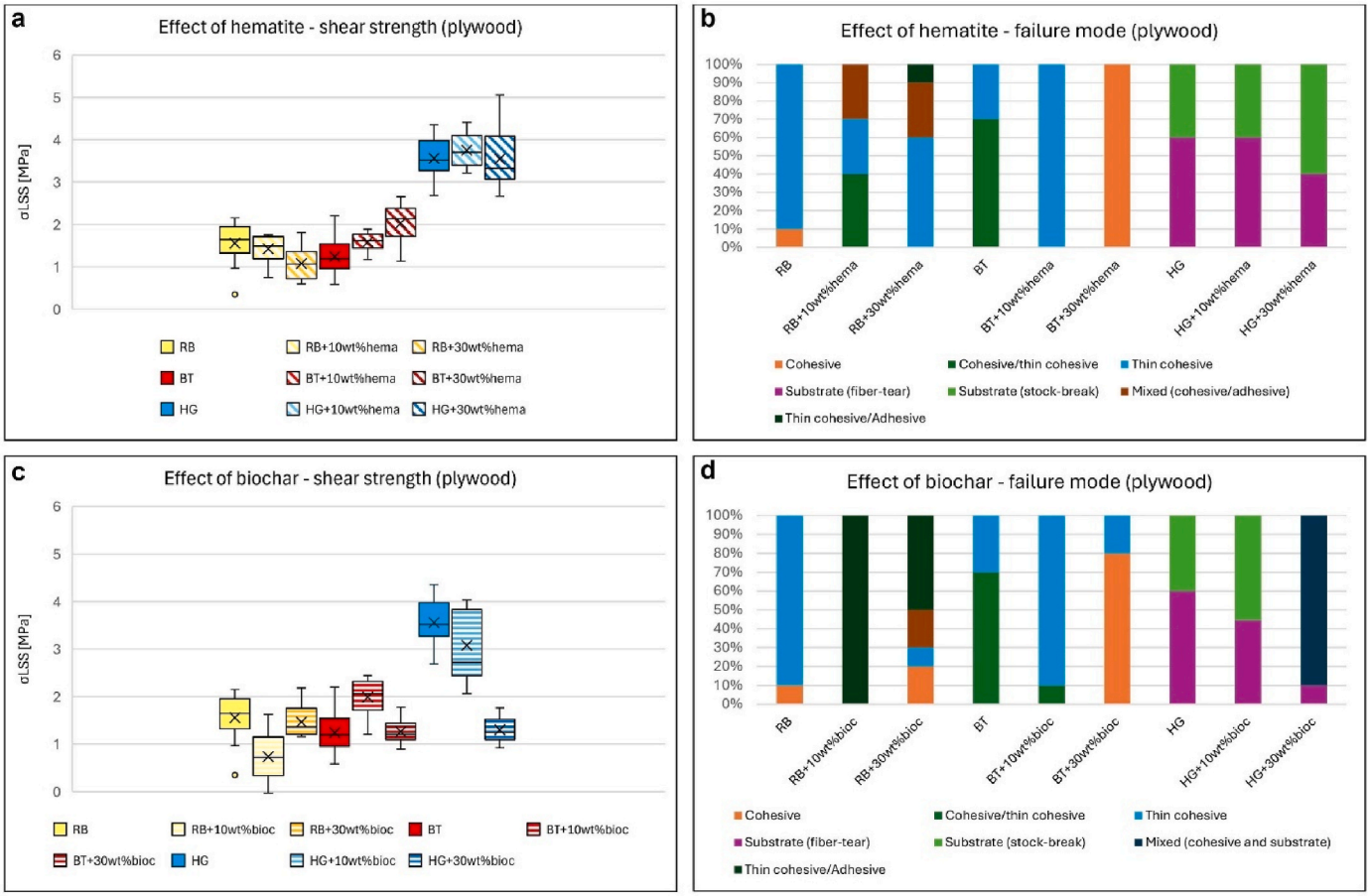

Fig. 7. Boxplot and stacked column graphs displaying the σLSS in MPa and failure modes (plywood) of archaeo-inspired adhesives with hematite (top) and biochar (bottom).

enhances thermal stability by increasing the degradation onset temperature. When 30 wt% hematite is added to the rosin-beeswax (7:3) blend, the onset temperature increases from ~270 °C to ~290 °C; the overall decomposition profile remains similar, but the mass loss curve becomes more gradual (Fig. 4a). The total mass loss is reduced accordingly, reflecting the non-volatile content of the sample (~30%). The degradation behaviour of the birch tar-hematite mixture is similar in shape to those of pure tar, but the degradation onset temperature shifted toward 300 °C, the slope is more gradual (Fig. 4b), and the residual mass again is substantially higher (~36%), consistent with the inorganic content added in this sample. Hematite-modified adhesives exhibit also an extended useable temperature range and could be safely used up to approximately 170–190 °C.

The addition of 30 wt% hematite to the rosin-beeswax (7:3) blend altered its thermal behaviour by lowering the melting temperature by approximately 10 °C, from 64 °C to 55 °C (Table 1). The enthalpy of melting of the mixture, corrected for the mass of the hematite, decreases strongly from 138 to 54.5 J/g, indicating that hematite disrupted the crystalline domains within the material.

Conversely, adding 30 wt% hematite to birch tar did not affect the melting temperature. The enthalpy of melting of the mixture, corrected for the mass of the hematite, increased from 51 to 64.5 J/g (Table 1), likely reflecting some increase of crystallinity.

3.2.4. Rheology and debonding temperatures

The debonding temperature of the rosin-beeswax (7:3) blend with 30 wt% hematite was 57.5 °C (Table 1), indicating that the addition of hematite particles does not significantly affect the debonding temperature compared to the unmodified blend (58 °C). In contrast, when hematite particles were added to birch tar, the debonding temperature decreased substantially from ca. 99 °C to 69 °C at 30 wt% hematite (Table 1), suggesting that hematite impacts birch tar debonding temperature.

3.3. Exploring birch tar reusability

3.3.1. Single lap-shear-joint (SLS) test

Fig. 9a shows the representative load-displacement curves of the CFRP composites bonded with tar containing 30 wt% hematite, as well as the same adhesive after one and five reheating cycles. As shown, the reference tar with 30 wt% hematite adhesive and the mixture reheated once exhibit largely comparable behaviour in the initial loading region, with nearly identical stiffness. Both curves display a steady increase in load with displacement, followed by a pronounced peak. The reheated-once mixture reaches the highest maximum force (slightly above 1000 N), exceeding the reference adhesive. In contrast, the adhesive reheated five times presents a markedly different response. While its initial stiffness is lower, a more gradual load increase is observed throughout the elastic region. The maximum force is significantly reduced, reaching only around 650–700 N. The birch tar +30 wt% hematite sample exhibited a mixed failure mode, comprising approximately 60% ductile and 40% brittle fracture. Upon reheating once, the failure shifted toward fully brittle behaviour. However, after five reheating cycles, the failure mode transitioned to fully ductile, accompanied by a notable decrease in peak load (Fig. S10).

Fig. 9b presents the joint's shear strength of CFRP composites. Reheating the birch tar with 30 wt% hematite mixture once led to a ~11% increase in the average lap shear strength (from 2.98 ± 0.44 MPa

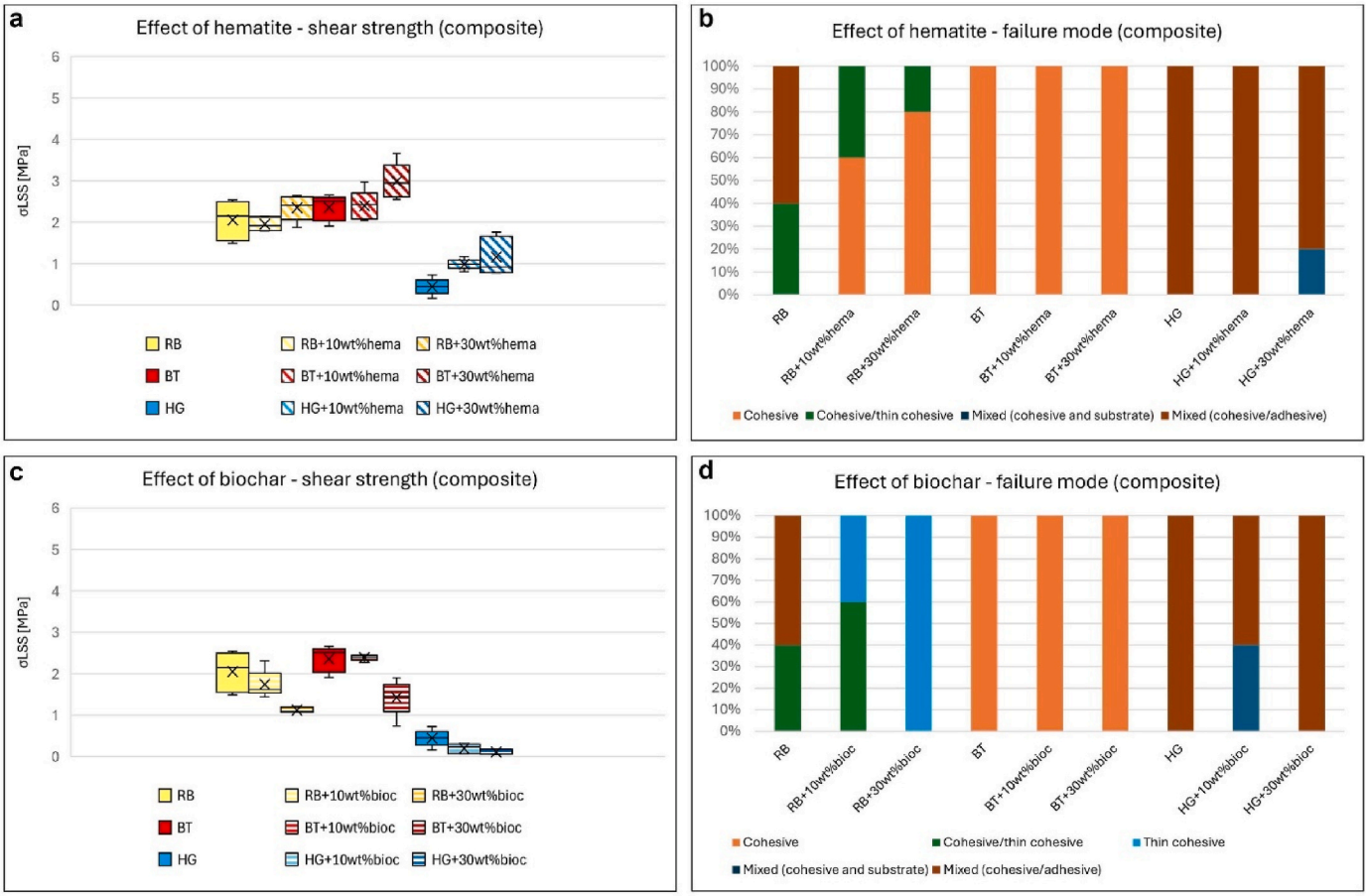

Fig. 8. Boxplot and stacked column graphs displaying the σLSS in MPa and failure modes (CFRP composites) of arche-inspired adhesives with hematite (top) and biochar (bottom).

to 3.30 ± 0.58 MPa, Table S10), whereas after five heating cycles, the average lap shear strength significantly decreased by ~28% (to 2.14 ± 0.31 MPa, *t*-test, $p < 0.01$). All samples exhibited cohesive failure (Fig. 9c, Fig. S3).

3.3.2. *Structural characterisation: X-ray diffraction (XRD)*

Fig. 10 presents the XRD patterns of birch tar and reheated tar samples, both with and without 30 wt% hematite. Across all samples, including those reheated once and five times, no significant phase changes are observed. The diffraction patterns show neither shifts in peak positions nor the emergence of new reflections, indicating that reheating and hematite addition do not alter the crystalline phases present.

The relative integrated intensities of the {021} Friedelin and Carnauba wax {102} reflections with respect to the integrated intensity of the hematite {104} reflection (taken as 100), showed a decrease after reheating the material (Fig. 11). The decrease in relative peak intensities suggests that both components lose some of their long-range ordered crystalline structure after each heating step.

3.3.3. *Thermal properties: thermogravimetric analysis (TGA)*

Reheating appears to enhance the thermal stability of both pure birch tar and tar-hematite mixtures (Fig. 4b). The sample of birch tar reheated once exhibits a slower decomposition rate and retains a higher residual mass (~20%) compared to unmodified tar (~5%) (Table 1). Repeated reheating further amplifies this effect, suggesting the formation of more thermally stable structures. The impact is even more pronounced in tar–hematite mixtures: both reheated variants show significantly reduced weight loss, with over 50% residue remaining after heating (Table 1).

In an effort to explain the effects of increased residue quantities, additional TGA measurements were performed on the same sample set as before, but this time under oxygen atmosphere instead of nitrogen atmosphere (Fig. 12). The oxygen flow would allow organic matter to combust, resulting in a solely inorganic residue. Both reheated birch tar samples (x1 and x5) show a similar degradation pattern, all resulting in minimal residue (~0%), indicating the presence of exclusively organic matter in the samples. The tar-hematite mixtures, however, present a different effect. The residual weight of the 1x reheated (~45%) and 5x reheated (~48%) samples show a defined increase of residue compared to the unmodified tar (~24%). Given that the analysis was performed in oxygen atmosphere, the residue was presumed to only contain inorganic matter, which was confirmed by XRD measurements (Fig. S11). Analyses performed on residue of the 5x reheated sample showed a mixture of only hematite and magnetite, originating from the added hematite.

Birch tar, both untreated and reheated showed only organic matter present in the sample. With the addition of hematite, the residual weight increased to 24%, the same as the measurement in nitrogen atmosphere. The increase of the residual weight of the reheated tar-hematite mixtures can therefore only be explained to be caused by a higher concentration of hematite in the original material.

3.3.4. *Fourier-transform infrared spectroscopy (FTIR)*

Fig. 13 shows the ATR-FTIR spectra of birch tar and birch tar mixed with 30 wt% hematite, including samples subjected to one and five reheating cycles. The principal absorption bands characteristic of birch tar –aliphatic C-H stretching (~2920 and 2850 cm^{-1}), carbonyl stretching (~1710–1740 cm^{-1}), aromatic skeletal vibrations

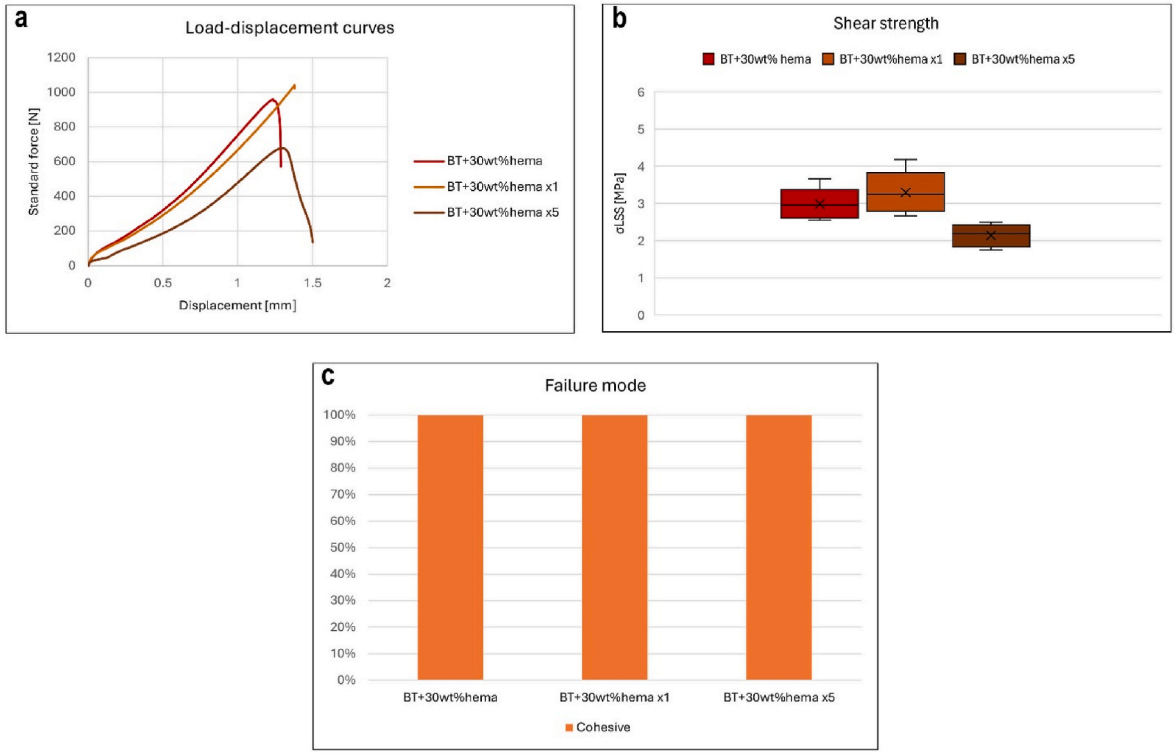

Fig. 9. a) load-displacement curves, b) shear strength, and c) failure modes representative of birch tar+30 wt%hematite and birch tar+30 wt%hematite reheated once and five times.

(~1600 cm^{-1}), and C-O stretching vibrations (1000–1400 cm^{-1})– are present in all samples. This indicates that the overall molecular framework of the tar is largely retained after reheating.

Closer inspection, however, reveals progressive modifications in specific spectral regions. In the carbonyl region, a doublet is observed around ~1710–1740 cm^{-1} in the unloaded tar (Fig. 13a). Upon reheating, subtle redistribution of intensity between the two components occurs. In the hematite-containing samples, repeated reheating enhances the higher-wavenumber contribution (~1730–1735 cm^{-1}) relative to the lower-wavenumber band (~1710–1715 cm^{-1}) (Fig. 13b), indicating modification of carbonyl functionalities. The increase of the band at 1733 cm^{-1} correlates with the increase of the band at 1167 cm^{-1}. This evolution may reflect degradation and oxidation processes induced by heating (cf. [22]) and potentially enhanced by the presence of hematite.

Minor attenuation and broadening are also visible in the C-O stretching region (1000–1400 cm^{-1}) after multiple reheating cycles. These variations are consistent with partial transformation or degradation of oxygenated biomarker components rather than the formation of new functional groups.

Variations in absolute band intensity between spectra should nevertheless be interpreted with caution. ATR-FTIR measurements are sensitive to sample-crystal contact, surface roughness, and effective penetration depth of the evanescent wave. The samples analysed here were small and exhibited heterogeneous, uneven surfaces, particularly in the mineral-containing mixtures. Differences in compaction, particle distribution, and surface conformity may therefore produce global intensity scaling across the spectrum without necessarily indicating compositional changes.

4. Discussion

4.1. Substrate-dependent adhesion

Wood substrates present a porous, hydrophilic, and hydroxyl-rich surface that facilitates adhesive penetration and hydrogen bonding [38]. Protein-based hide glue is known to form polar interactions and mechanical interlocking within lignocellulosic substrates, which explains the substrate failure observed in plywood specimens bonded with hide glue and, consequently, the higher lap shear strength values.

On the other hand, CFRP substrates present a lower surface energy and are less chemically reactive. Adhesion on CFRP substrates will strongly depend on the surface activation, compatibility between adhesive and epoxy matrix used on the CFRP and mechanical interlocking [32].

It was observed that birch tar's superior performance on CFRP relative to hide glue likely derives from its thermoplastic, conformable nature, enabling improved wetting and interfacial contact under pressure. The transition toward cohesive failure in tar-bonded CFRP joints suggests that interfacial adhesion exceeded the internal cohesive strength, indicating effective surface adhesion.

4.2. Usability, debondability, and reusability of the archaeo-inspired bio-based adhesives examined

4.2.1. Usability

The maximum average lap shear strengths of the archaeo-inspired adhesives tested ranged from 1.5 to 3.5 MPa –making them suitable for light-duty, non-structural applications requiring moderate mechanical performance– and are consistent with values reported for other bio-based adhesives (e.g., Ref. [39–41]). Direct comparison with published data on the same adhesives is difficult, particularly for birch tar, whose strength strongly depends on production methods; nevertheless, our values fall within the ranges reported in the literature [7,9,10,19] (see

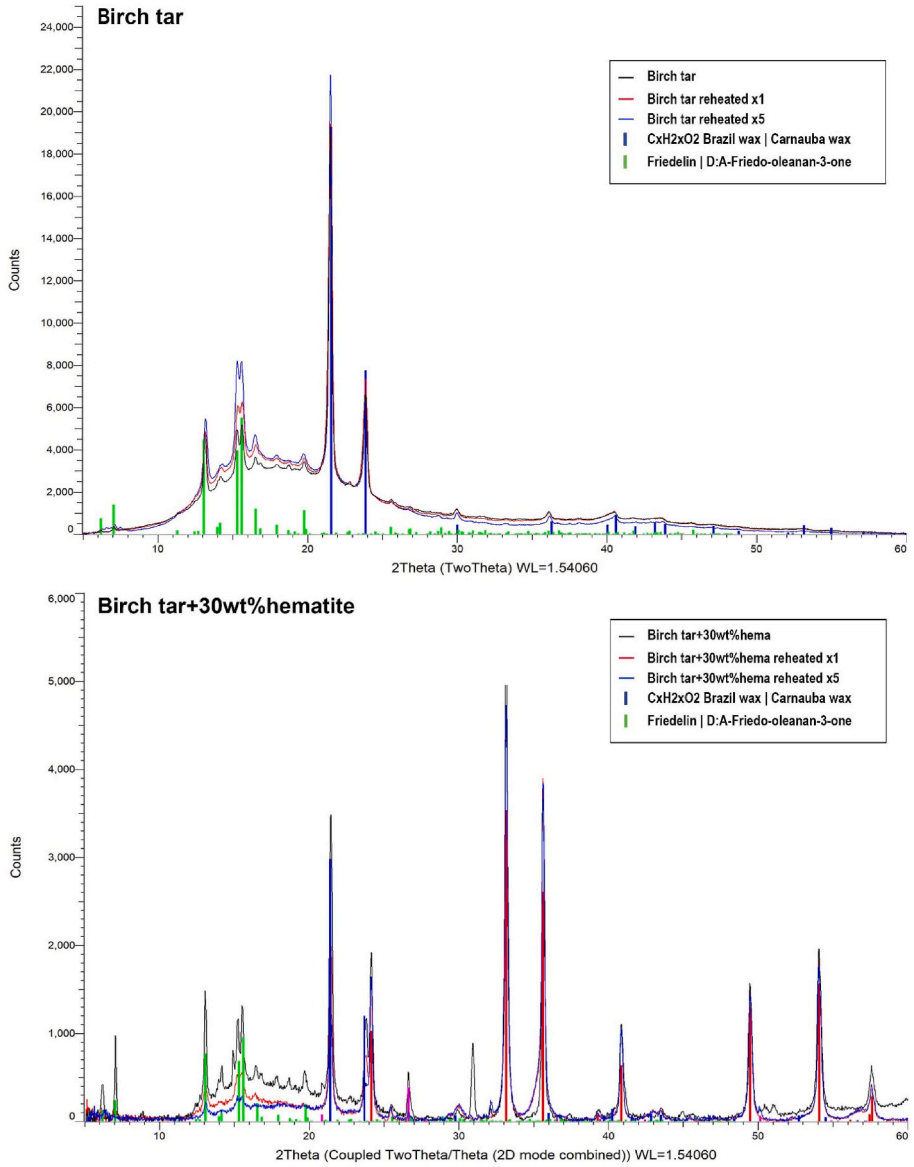

Fig. 10. XRD patterns of tar and reheated tar samples (top) and tar+30 wt%hematite and reheated tar+30 wt%hematite samples (bottom).

SI4).

Comparisons can, however, be made with other bio-based formulations studied in recent years for wood applications, which also appear to be the most plausible application the adhesive studied here. Soy protein-based adhesives typically exhibit average lap shear strengths between 0.6 and 1.2 MPa, but under optimised conditions or with modifiers can reach 2.8–3.0 MPa [42–44]. Fully bio-based lignin adhesives generally show average lap shear strengths of 1.0–1.4 MPa, while chemically modified lignins can achieve up to 5 MPa [45,46]. Tannin and tannin-hybrid adhesives show similar values, ranging approximately from 0.7 to 2.4 MPa [47–49].

4.2.2. *Filler effect: reinforcement versus defect introduction*

Hematite generally improved the average lap shear strength across all three adhesives, most notably in birch tar, where increases reached 64% on wood (from 1.24 ± 0.45 to 2.03 ± 0.49 MPa) and 27% on CFRP composites (from 2.35 ± 0.31 to 2.98 ± 0.44 MPa). Compared with previous studies [7,16,50], the rosin-beeswax-hematite blend, however, showed lower average lap shear strength on plywood, likely due to differences in mineralogy, particle size, and distribution of the red ochre, as well as in adherend surface roughness.

Importantly, our experiments provide the first direct evidence that hematite enhances the performance of birch tar, suggesting broader applicability as a reinforcement in natural adhesives.

XRD and mechanical results reveal clear structure-property relationships in the hematite-filled bio-based adhesives. Indeed, fine mineral particles, such as hematite, can enhance stiffness and apparent cohesive strength via crack deflection, thereby enhancing energy dissipation, load transfer from the deformable matrix to the high-modulus filler phase, and restriction of local deformation within the bond line. SEM analysis indicates that hematite particles were finely divided and homogeneously dispersed, promoting effective interfacial load transfer and minimising stress concentration sites (see Fig. 14(c) and (d)).

However, filler addition can also increase brittleness if particle dispersion is suboptimal, as with biochar, or if the matrix is already relatively crystalline, as with rosin-beeswax blends.

Conversely, biochar generally reduced the average lap shear strength. Fig. 14 compares the microstructural characteristics of adhesives loaded with biochar and hematite, highlighting differences in particle size, morphology, and dispersion within the adhesive matrix. Biochar-filled adhesives exhibit relatively large, irregular particles and pronounced agglomeration, whereas hematite is more finely divided

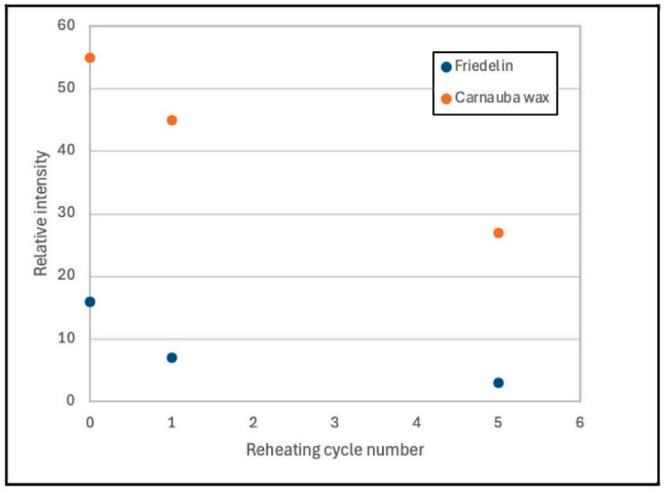

Fig. 11. Reduction of intensities of the {021} of Friedelin and {102} of Carnauba wax as a function of reheating cycles, suggesting a loss of crystallinity. Intensities are relative to the hematite {104} intensity (taken as 100).

and more homogeneously distributed, despite both fillers being mixed under the same conditions. The inherently larger size and irregular morphology of biochar particles likely contribute to these agglomerates, which reduce adhesive strength, particularly at 30 wt%, due to its larger particle size and high volume fraction, which overload the matrix and hinder effective stress transfer, in agreement with previous observations on charcoal fillers [29].

Future work should aim to decouple these effects by systematically controlling particle size across different filler types, for example by using comparable grain size distributions or by further processing the fillers. In addition, strategies such as mechanical mixing, surfactants, or chemical modification could be explored to improve particle dispersion and potentially enhance adhesive performance.

Birch tar mixtures exhibited broad interfacial compatibility, bonding porous and nonporous substrates such as wood, composites, and –based on literature– aluminium and stone [10,29]. Rosin-beeswax mixtures also adhered well to plywood and CFRP composites. In contrast, hide glue performed notably better on wood than on CFRP composites (σLSS = 3.56 ± 0.49 MPa vs. 0.44 ± 0.20 MPa), in line with its reliance on polar amino acid interactions [51].

4.2.3. Moisture resistance

Birch tar and rosin-beeswax mixtures are water-insoluble, and their hydrophobic composition makes them potentially suitable for indoor and outdoor use. Their performance under exterior conditions, however, still requires verification through standard tests assessing resistance to moisture, temperature fluctuations, and UV exposure. In contrast, hide glue shows poor water resistance and is highly susceptible to biodegradation. Protein-based adhesives can be improved through chemical or enzymatic modification or by blending with oils or resin acids [4,52,53].

Although further testing is needed, previous work [54] suggests that hematite may enhance the water resistance of gum-based adhesives. Hematite also exhibits antibacterial properties and can inhibit microbial collagenase activity [55–57], consistent with its historical role as a tanning agent. Thus, hematite may simultaneously improve shear strength, water resistance, and biodegradation stability.

4.2.4. Thermal behaviour and debondability

Thermal stability of birch tar is higher than rosin and rosin-beeswax blend, with decomposition onsetting at ~275 °C compared to ~200–250 °C for rosin and ~270 °C for the blend. The ability to debond these systems by heating situates them within the broader category of thermally reversible or debondable adhesives.

Hematite incorporation significantly alters the thermal behaviour of the adhesives. In both rosin-beeswax and birch tar systems, TGA showed a delayed onset of degradation and higher residual char, indicating enhanced thermal stability due to the inorganic filler. The onset of mass loss increased from ~270 °C to ~290 °C in the rosin-beeswax blend and from ~275 °C to ~300 °C in birch tar. In polymer-filler composites, such improvements commonly arise because inorganic particles act as thermally inert domains that redistribute heat locally and hinder the mobility and decomposition of the organic matrix. Consistent with this behaviour, hematite addition increases stiffness and crystallinity while improving thermal stability; however, the accompanying rise in rigidity may limit ductility.

As sustainability and reparability gain prominence, the ability to reversibly debond adhesives has become a key design consideration [58]. Since both rosin and tar are thermoplastic, they can be reversibly softened and detached by heating above their melting or softening point while applying mechanical loads. Our rheological measurements demonstrated that hematite promotes more efficient thermo-mechanical debonding in birch tar: adding 30 wt% hematite reduced the debonding temperature by approximately 30 °C (from 99 °C to 69 °C; Table 1). The notable reduction in debonding temperature upon hematite addition to birch tar suggests potential changes in thermal transport and yielding

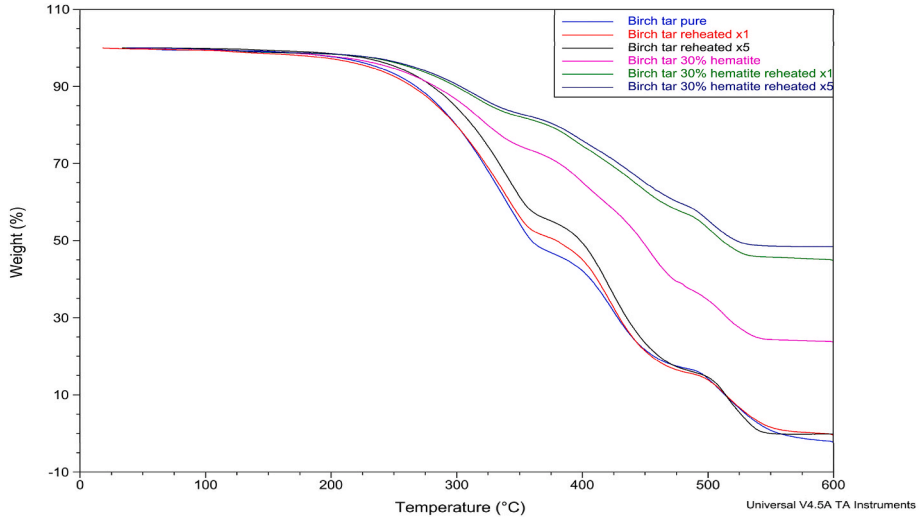

Fig. 12. TGA curves displaying the weight loss (%) of birch tar blends during heating from 0 °C to 600 °C in oxygen atmosphere.

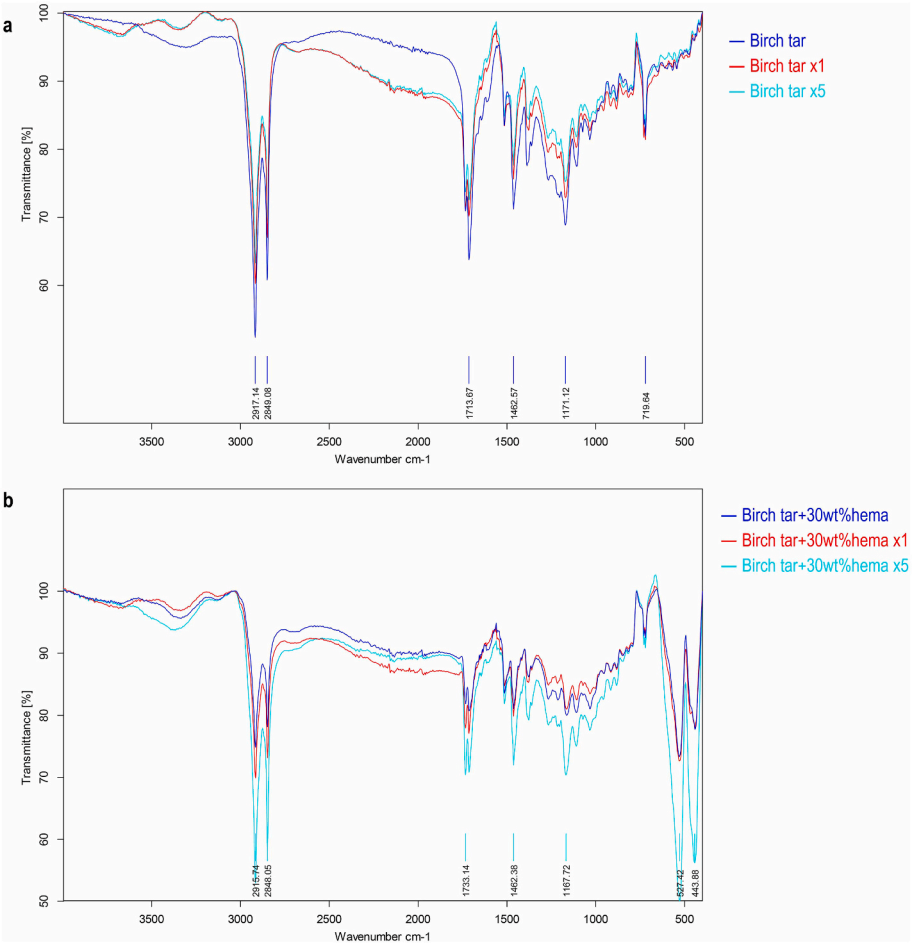

Fig. 13. ATR-FTIR spectra of (a) tar and reheated tar samples and (b) tar+30 wt%hematite and reheated tar+30 wt%hematite samples.

behaviour. Inorganic fillers commonly increase thermal conductivity in polymer composites, accelerating heat transfer through the adhesive layer and potentially lowering the practical temperature required for interfacial softening [59].

By contrast, hematite reduced the melting temperature but not the debonding temperature of the rosin-beeswax blend (Table 1), reflecting differences in chemical compatibility between filler and matrix. Birch tar contains polar phenolic and aromatic compounds [21,60] capable of interacting with hematite particles, whereas rosin and beeswax are mainly composed of non-polar esters and fatty acids [35], resulting in weaker filler-matrix coupling. Nevertheless, hematite addition decreased the melting enthalpy of the rosin-beeswax adhesive, suggesting that filler incorporation disrupts molecular packing and lowers the energy required for melting or recycling (cf. [61,62]).

Overall, hematite modifies both the thermal stability and debonding behaviour of these bio-based adhesives. It enhances degradation resistance and energy efficiency, supporting the development of thermally tuneable and recyclable adhesive systems. However, its use should be balanced against the increased stiffness and reduced ductility that may limit performance in flexible or long-term structural applications.

4.2.5. *Reusability*

Birch tar behaves like a thermoplastic: it softens when heated and hardens upon cooling without chemical phase change, allowing repeated use through reheating [63].

Interestingly, after one reheating cycle (~10 min), the tar-hematite mixture showed an 11% average lap shear strength increase compared to the non-reheated sample (from 2.98 ± 0.44 to 3.30 ± 0.58 MPa). This strengthening suggests that limited thermal exposure promotes beneficial structural rearrangements within the adhesive layer. Because FTIR, XRD, and TGA analyses revealed no new chemical phases or measurable changes in crystallinity (Figs. 10 and 13), the improvement cannot be attributed to bulk chemical crosslinking. Instead, it is more plausibly explained by physical reorganisation processes, including: (i) enhanced wetting and interfacial contact due to temporary viscosity reduction, (ii) densification of the adhesive layer via relaxation of entrapped voids, (iii) improved filler dispersion or particle–matrix packing efficiency, and potentially, (iv) molecular-level rearrangement leading to increased cohesive packing density.

Such heat-induced densification and defect relaxation are documented in thermoplastic and pitch adhesives, where short processing intervals can enhance mechanical performance before thermal degradation becomes dominant [29].

The subsequent 28% strength reduction after five reheating cycles (~20 min cumulative heating; 2.14 ± 0.31 MPa, $p < 0.05$) indicates that prolonged thermal exposure shifts the balance toward degradation mechanisms. Previous experimental archaeology studies on tar and pitch adhesives similarly report initial strengthening followed by performance decline with extended heating [10,29]. These declines can be attributed to thermally induced microstructural rearrangement, embrittlement from compositional fractionation, and disruption of optimal filler-matrix interactions.

The absence of new FTIR bands or crystallographic transitions suggests that degradation remains primarily microstructural rather than chemical, occurring below the detection threshold of bulk spectroscopy and diffraction.

Correlating these results with lap shear tests suggests that initial reheating induced molecular rearrangements –such as crosslinking or

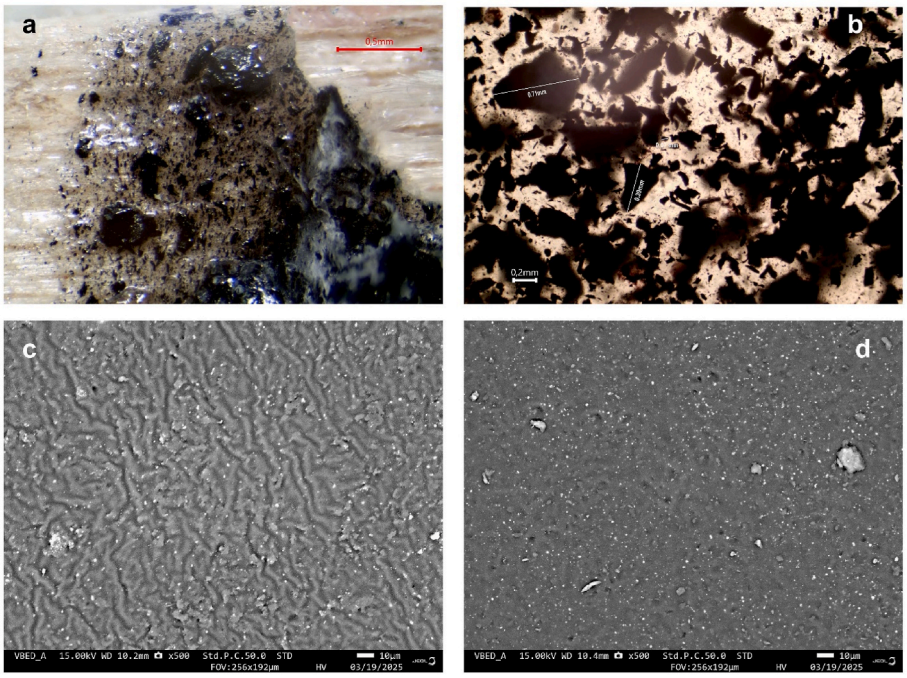

Fig. 14. Comparison between adhesives loaded with biochar (top) and hematite (bottom), showing differences in particle size and distribution. A) Stereomicroscope image of a hide glue adhesive mixed with biochar on the fracture surface of a lap shear sample, showing visible biochar agglomerates (40x); b) transmitted light microscopy image of a rosin-beeswax blend loaded with biochar, showing particle distribution and size variation (30x); c) SEM image of birch tar adhesive containing 10 wt% hematite and d) with 30 wt% hematite (500x) showing particle size and dispersion.

polymer network compaction– that improved strength and stability. These effects may have been favoured by hematite, as fillers can influence the behaviour of polymer networks [64,65]. Consequently, tar-hematite reheated once exhibited greater stiffness and strength, with fracture behaviour shifting from ductile to brittle (Table S10). By contrast, repeated reheating caused structural damage, loss of strength, and reversion from brittle to ductile fracture behaviour.

4.2.6. *Applicability-specifics*

In summary, adhesive suitability is application-specific, and some considerations can be made for each studied adhesive.

- Hide glue delivers the highest strength on wood and is therefore best suited for wood-wood structural bonding under dry indoor conditions, though its moisture sensitivity limits broader use.
- Birch tar demonstrates the widest substrate compatibility, including effective bonding to CFRP, along with thermoplastic debondability and reusability, making it particularly promising for multi-material assemblies and circular design strategies that require repair or thermal disassembly.
- Rosin-beeswax blends provide moderate performance but exhibit greater brittleness and substrate sensitivity, restricting their use to light-duty or temporary applications.

4.3. *Future directions*

In summary, hematite has emerged as an effective additive, significantly enhancing lap shear strength and thermal properties, particularly in birch tar formulations.

Beyond the performance improvements achieved with hematite, several areas for further development remain within the adhesive systems studied.

- The high biochar loading reduces mechanical performance, indicating that optimisation of both biochar particle size and filler content is essential for improving bio-based adhesive formulations.
- The limited water resistance and biodegradability of hide glue remain limiting factors, necessitating further exploration of chemical modifications or alternative additives. Hematite appears to be a promising filler for improving the water resistance of protein-based glues; however, targeted testing protocols are required to validate this potential.
- The mechanisms underlying tar degradation during repeated reheating are not fully understood, suggesting that further studies are needed to identify the causes of performance loss and potential strategies to mitigate it.

Future research should focus on optimising filler content, particle size, and matrix compatibility to improve the mechanical and functional performance of these adhesives. Once adequate performance is achieved, sustainability assessments such as preliminary or full life cycle analyses (LCAs) can be conducted to quantify their environmental footprint. Addressing these aspects will further advance the practical applicability and sustainability credentials of archaeo-inspired adhesives, enhancing their relevance and competitiveness within the modern bio-based adhesive sector.

5. Conclusion

This study examined the performance and potential of archaeo-inspired bio-based adhesives –birch tar, rosin-beeswax blends, and hide glue– modified with natural additives such as hematite and biochar. Using a multi-analytical approach, we systematically characterised their bonding performance, debondability, and reusability, providing a comprehensive dataset to support the development of sustainable adhesives. Archaeological knowledge, combined with systematic material characterisation, informs the design principles of renewable adhesives based on natural feedstocks or by-products.

The three adhesives demonstrated average lap shear strengths between 1.5 and 3.5 MPa, positioning them as viable candidates for light-duty, non-structural applications. Birch tar exhibited the broadest substrate compatibility and the highest reuse potential, with hematite enhancing shear strength and lowering debonding temperature, supporting energy-efficient, reversible applications; performance declined after multiple reheating cycles, indicating thermally induced rearrangements. Hide glue achieved the highest lap shear strength on wood but showed poor water resistance and limited performance on nonporous substrates. Rosin-beeswax blends demonstrated balanced bonding on wood and composite substrates, with moderate moisture resistance and thermo-mechanical debondability, suitable for reversible applications.

Hematite consistently improved mechanical and thermal properties across adhesives, while biochar reduced strength at higher loadings, likely due to particle size and volume fraction effects. Hematite thus emerges as a dual-function additive, enhancing performance while maintaining debondability, supporting the development of repairable, recyclable bio-based systems.

These findings demonstrate the viability of natural adhesives for sustainable bonding strategies, particularly where disassembly and reuse are important. The dataset generated provides a foundation for future studies on filler optimisation, long-term durability, biodegradation, and scale-up feasibility, advancing next-generation sustainable adhesives.

Declaration of generative AI and AI-assisted technologies in the writing process

During the preparation of this work, the authors used ChatGPT (OpenAI, GPT-5.2) to check the grammar, spelling, and improve the readability of the text. After using this tool, the authors reviewed and edited the content as needed and take full responsibility for the content of the published article.

Funding

The BiDebA project (ID: NWE0300399) has received funding from the European program Interreg North-West Europe.

CRediT authorship contribution statement

A. Aleo: Conceptualization, Data curation, Formal analysis, Investigation, Methodology, Validation, Visualization, Writing – original draft, Writing – review & editing. **R. de Araujo Alves Lima:** Conceptualization, Data curation, Formal analysis, Investigation, Methodology, Validation, Writing – original draft, Writing – review & editing. **D. Molendijk - van den Hengst:** Data curation, Formal analysis, Investigation, Visualization, Writing – original draft, Writing – review & editing. **R.W.A. Hendrikx:** Formal analysis, Investigation, Writing – review & editing. **S. Teixeira de Freitas:** Conceptualization, Supervision, Writing – review & editing. **G.H.J. Langejans:** Conceptualization, Funding acquisition, Methodology, Supervision, Writing – review & editing. **A.J. Böttger:** Conceptualization, Funding acquisition, Investigation, Methodology, Supervision, Validation, Writing – original draft, Writing – review & editing.

Declaration of competing interest

The authors declare that they have no known competing financial interests or personal relationships that could have appeared to influence the work reported in this paper.

Acknowledgments

We thank our colleagues from the project partner organizations – Flanders Make (Belgium), Avans Hogeschool (The Netherlands), GMI (France), and Acrats (The Netherlands)– for their valuable feedback and support during the testing of the archaeo-inspired adhesives. We also extend our gratitude to the colleagues at TU Delft (The Netherlands), particularly from the Faculty of Mechanical Engineering and the Faculty of Aerospace Engineering, for facilitating access to laboratories and other facilities during the adhesives' manufacturing and testing phases. We thank Radhey Bachhav and Kees Kwakernaak (Faculty of Mechanical Engineering, TU Delft) for their support during the acquisition of SEM images; Davide Biagini and Zhiyuan Xu (Faculty of Aerospace Engineering, TU Delft) for their help during sample preparation. Authors R. de Araujo Alves Lima and S. Teixeira de Freitas acknowledge Fundação para a Ciência e a Tecnologia (FCT), Portugal, for its financial support via LAETA (project https://doi.org/10.54499/UID/50022/2025.

Appendix A. Supplementary data

Supplementary data to this article can be found online at https://doi.org/10.1016/j.ijadhadh.2026.104387.

Data availability

All data supporting the findings of this study are available within the manuscript and its Supplementary Information

References

[1] Banea MD, da Silva LFM, Campilho RDSG, Sato C. Smart adhesive joints: an overview of recent developments. J Adhes 2014;90(1):16–40. https://doi.org/10.1080/00218464.2013.785916.
[2] Budhe S, Banea MD, de Barros S, da Silva LFM. An updated review of adhesively bonded joints in composite materials. Int J Adhesion Adhes 2017;72:30–42. https://doi.org/10.1016/j.ijadhadh.2016.10.010.
[3] Lima RAA, Tao R, Bernasconi A, Carboni M, Carrere N, De Freitas ST. Uncovering the toughening mechanisms of bonded joints through tailored CFRP layup. Compos B Eng 2023;263:110853. https://doi.org/10.1016/j.compositesb.2023.110853.
[4] Islam MN, Rahman F, Das AK, Hiziroglu S. An overview of different types and potential of bio-based adhesives used for wood products. Int J Adhesion Adhes 2022;112:102992. https://doi.org/10.1016/j.ijadhadh.2021.102992.
[5] Westerman CR, McGill BC, Wilker JJ. Sustainably sourced components to generate high-strength adhesives. Nature 2023;621(7978):306–11. https://doi.org/10.1038/s41586-023-06335-7.
[6] Langejans G, Aleo A, Fajardo S, Kozowyk P. Archaeological adhesives. Oxford Research Encyclopedia of Anthropology 2022. https://doi.org/10.1093/acrefore/9780190854584.013.198.
[7] Kozowyk PRB, Langejans GHJ, Poulis JA. Lap shear and impact testing of ochre and beeswax in experimental Middle Stone Age compound adhesives. PLoS One 2016;11(3):e0150436. https://doi.org/10.1371/journal.pone.0150436.
[8] Kozowyk PRB, Poulis JA. A new experimental methodology for assessing adhesive properties shows that Neandertals used the most suitable material available. J Hum Evol 2019;137:102664. https://doi.org/10.1016/j.jhevol.2019.102664.
[9] Schmidt P, Blessing MA, Koch TJ, Nickel KG. On the performance of birch tar made with different techniques. Heritage Science 2021;9(1):140. https://doi.org/10.1186/s40494-021-00621-1.
[10] Schmidt P, Koch TJ, Berthold C, Lauxmann F, Nickel KG. The evolution of strength, elasticity and rupture behaviour of birch tar made with 'double-pot' techniques during tar cooking. Archaeometry 2022. https://doi.org/10.1111/arcm.12820.
[11] Wadley L. Compound-Adhesive manufacture as a behavioral proxy for complex cognition in the Middle Stone Age. Curr Anthropol 2010;51(S1):S111–9. https://doi.org/10.1086/649836.
[12] Gupta S, Kua HW, Koh HJ. Application of biochar from food and wood waste as green admixture for cement mortar. Sci Total Environ 2018;619–620:419–35. https://doi.org/10.1016/j.scitotenv.2017.11.044.
[13] Bartoli M, Arrigo R, Malucelli G, Tagliaferro A, Duraccio D. Recent advances in biochar polymer composites. Polymers 2022;14(12).
[14] Kępniak M, Załęgowski K, Woyciechowski P, Pawłowski J, Nurczyński J. Feasibility of using biochar as an eco-friendly microfiller in polymer concretes. Polymers 2022;14.
[15] Elvers B, Rounsaville JF, Schulz G, Ullman F. Ullmann's encyclopedia of industrial chemistry, vol. 23. Wiley-VCH; 1989. 5th edition (V ed.
[16] Gaillard Y, Chesnaux L, Girard M, Burr A, Darque-Ceretti E, Felder E, Mazuy A, Regert M. Assessing hafting adhesive efficiency in the experimental shooting of projectile points: a new device for instrumented and ballistic experiments. Archaeometry 2016;58(3):465–83. https://doi.org/10.1111/arcm.12175.
[17] Luan Q-f, Tao X-y, Diao S, Ding X-y, Jiang J-m. Chapter 6 - methods, characteristics, variance, and genetics of pine oleoresin components, and their potential for renewable and sustainable energy. In: Atta ur R, editor. Studies in

natural products chemistry, vol. 68. Elsevier; 2021. p. 221–53. https://doi.org/10.1016/B978-0-12-819485-0.00018-9.
[18] Gaillard Y, Mija A, Burr A, Darque-Ceretti E, Felder E, Sbirrazzuoli N. Green material composites from renewable resources: polymorphic transitions and phase diagram of beeswax/rosin resin. Thermochim Acta 2011;521(1):90–7. https://doi.org/10.1016/j.tca.2011.04.010.
[19] Schmidt P, Blessing M, Rageot M, Iovita R, Pfleging J, Nickel KG, Righetti L, Tennie C. Birch tar production does not prove Neanderthal behavioral complexity. Proc Natl Acad Sci U S A 2019;116(36):17707–11. https://doi.org/10.1073/pnas.1911137116.
[20] Regert M. Investigating the history of prehistoric glues by gas chromatography–mass spectrometry. J Separ Sci 2004;27(3):244–54. https://doi.org/10.1002/jssc.200301608.
[21] Rageot M, Théry-Parisot I, Beyries S, Lepère C, Carré A, Mazuy A, Filippi J-J, Fernandez X, Binder D, Regert M. Birch bark tar production: experimental and biomolecular approaches to the Study of a common and widely used prehistoric adhesive. J Archaeol Method Theor 2019;26(1):276–312. https://doi.org/10.1007/s10816-018-9372-4.
[22] Schmidt P, Koch TJ. The molecular composition of birch tar and its infrared spectrum. Anthropological and Archaeological Sciences 2024;19:153. https://doi.org/10.1007/s12520-024-02102-5.
[23] Marsh P. *Biocoal fuel product and processes and systems for the production thereof* (United States Patent No. USPTO. 2021. https://www.freepatentsonline.com/10995274.html.
[24] Negash TG, Emiru A, Amare D, Reda M. Production and characterization of glue from tannery hide trimming waste. Adv Sci Technol 2020. Cham.
[25] Pearson CL. Animal glues and adhesives. In: Pizzi A, Mittal KL, editors. Handbook of adhesive technology. second ed. ed. Marcel Dekker Inc; 2003. p. 479–94.
[26] Kan T, Strezov V, Evans TJ. Lignocellulosic biomass pyrolysis: a review of product properties and effects of pyrolysis parameters. Renew Sustain Energy Rev 2016;57:1126–40. https://doi.org/10.1016/j.rser.2015.12.185.
[27] Hodgskiss T. Ochre use in the Middle Stone Age. Oxford University Press; 2020.
[28] Edwards WP. Why not period glue? Journal of the Society of American Period Furniture Makers; 2001.
[29] Kozowyk PRB, Poulis JA, Langejans GHJ. Laboratory strength testing of pine wood and birch bark adhesives: a first Study of the material properties of pitch. J Archaeolog Sci: Rep 2017;13:49–59. https://doi.org/10.1016/j.jasrep.2017.03.006.
[30] International Organization for Standardization (ISO). ISO 4587:2003—Adhesives—Determination of tensile lap-shear strength of rigid-to-rigid bonded assemblies. 2003. Geneva, Switzerland.
[31] Rudawska A. 9 - assessment of surface preparation for the bonding/adhesive technology. In: Rudawska A, editor. Surface treatment in bonding technology. Academic Press; 2019. p. 227–75. https://doi.org/10.1016/B978-0-12-817010-6.00009-6.
[32] Teixeira de Freitas S, Dimitrios Z, Poulis JA. The use of acoustic emission and composite peel tests to detect weak adhesion in composite structures. J Adhes 2018;94(9):743–66. https://doi.org/10.1080/00218464.2017.1396975.
[33] Schellmann NC. Animal glues: a review of their key properties relevant to conservation. Stud Conserv 2007;52(sup1):55–66. https://doi.org/10.1179/sic.2007.52.Supplement-1.55.
[34] Schmidt P, Koch TJ, February E. Archaeological adhesives made from Podocarpus document innovative potential in the African Middle Stone Age. Proc Natl Acad Sci 2022;119(40):e2209592119. https://doi.org/10.1073/pnas.2209592119.
[35] Cavallaro G, Lazzara G, Milioto S, Parisi F, Sparacino V. Thermal and dynamic mechanical properties of beeswax-halloysite nanocomposites for consolidating waterlogged archaeological woods. Polym Degrad Stabil 2015;120:220–5. https://doi.org/10.1016/j.polymdegradstab.2015.07.007.
[36] Orsini S, Ribechini E, Modugno F, Klügl J, Di Pietro G, Colombini MP. Micromorphological and chemical elucidation of the degradation mechanisms of birch bark archaeological artefacts. Heritage Science 2015;3(1):2. https://doi.org/10.1186/s40494-015-0032-7.
[37] ASTM International. ASTM E2550-21 Standard Test method for thermal stability by thermogravimetry. West Conshohocken, PA: ASTM International; 2021. https://doi.org/10.1520/E2550-21.
[38] Xu W, Pranovich A, Uppstu P, Wang X, Kronlund D, Hemming J, Öblom H, Moritz M, Preis M, Sandler N, Willför S, Xu C. Novel biorenewable composite of wood polysaccharide and polylactic acid for three dimensional printing. Carbohydrate polymers 2018;187:51–8.
[39] Cheng HN, Dowd MK, He Z. Investigation of modified cottonseed protein adhesives for wood composites. Ind Crop Prod 2013;46:399–403. https://doi.org/10.1016/j.indcrop.2013.02.021.
[40] Li D, Ye X, Li Z, Huang S, Zhao R, Ma X, Li J, Yin F. Plant venation-inspired bio-based adhesive with toughness, wide temperature adaptability, and long-term adhesion. Chem Eng J 2025;508:160996. https://doi.org/10.1016/j.cej.2025.160996.
[41] Soubam T, Gupta A, Jamari SS. Eco-friendly bio-based adhesive for plywood from natural rubber latex (NRL)-blended isocyanate cross-linked starch. Environ Sci Pollut Control Ser 2023;30(60):124610–8. https://doi.org/10.1007/s11356-022-20788-9.
[42] Huang X, Chen Y, Lin X, Li J, Gao Q. A strong soy protein-based adhesive with excellent water retention. Chem Eng J 2023;472:145037. https://doi.org/10.1016/j.cej.2023.145037.
[43] Li M, Bai F, Cheng Y, Cao X, Guan E, Bian K. Study on adhesive properties of soybean meal-based adhesives modified by ultrasonic-chemical treatment. Int J Adhesion Adhes 2022;118:103237. https://doi.org/10.1016/j.ijadhadh.2022.103237.
[44] Zheng P, Zeng Q, Lin Q, Fan M, Zhou J, Rao J, Chen N. Investigation of an ambient temperature-curable soy-based adhesive for wood composites. Int J Adhesion Adhes 2019;95:102429. https://doi.org/10.1021/acsapm.0c01295.
[45] Siahkamari M, Emmanuel S, Hodge DB, Nejad M. Lignin-glyoxal: a fully biobased formaldehyde-free wood adhesive for interior engineered wood products. ACS Sustainable Chem Eng 2022;10(11):3430–41. https://doi.org/10.1021/acssuschemeng.1c06843.
[46] Yuan Jiafeng, Du Guanben, Yang Hongxing, Liu Sichen, Park Seongsu, et al. Fully bio-based adhesive designed through lignin-cellulose combination and interfacial bonding reinforcement. Industrial Crops and Products 2023;204:117279. https://doi.org/10.1016/j.indcrop.2023.117279. https://linkinghub.elsevier.com/retrieve/pii/S0926669023010440.
[47] Jiang S, Liu S, Du G, Wang S, Zhou X, Yang J, Li T. Chitosan-tannin adhesive: fully biomass, synthesis-free and high performance for bamboo-based composite bonding. Int J Biol Macromol 2023;230:123115. https://doi.org/10.1016/j.ijbiomac.2022.123115.
[48] Xu G, Zhang Q, Xi X, Lei H, Cao M, Du G, Wu Z. Tannin-based wood adhesive with good water resistance crosslinked by hexanediamine. Int J Biol Macromol 2023;234:123644. https://doi.org/10.1016/j.ijbiomac.2023.123644.
[49] Yang H, Du G, Ni K, Liu T, Su H, Wang H, Yang L. Sucrose-tannin-nanosilica hybrid bio-adhesive based on dual dynamic schiff base and disulfide bonds with enhanced toughness and cohesion. Int J Biol Macromol 2023;253:126672. https://doi.org/10.1016/j.ijbiomac.2023.126672.
[50] Wadley L. Putting ochre to the test: replication studies of adhesives that may have been used for hafting tools in the Middle Stone Age. J Hum Evol 2005;49(5):587–601. http://www.sciencedirect.com/science/article/B6WJS-4GYNY0K-2/2/41ce4c89fa2f95138de0f6960e1c5718.
[51] Conner A. Wood: adhesives. Encyclopedia of materials: science and technology. Amsterdam. New York: Elsevier Science, Ltd.; 2001. c2001.
[52] Oni OV, Lawrence MA, Zappi ME, Chirdon WM. A review of strategies to enhance the water resistance of green wood adhesives produced from sustainable protein sources. Sustainability 2023;15(20).
[53] Xu Y, Han Y, Li J, Luo J, Shi SQ, Li J, Gao Q, Mao A. Research progress of soybean protein adhesive: a review. J Renew Mater 2022;10(10):2519–41. https://doi.org/10.32604/jrm.2022.020750.
[54] Kozowyk PRB, Langejans GHJ. Form of function? An experimental study on the role of fillers in Stone Age compound adhesives. In: Abstracts of 14th annual meeting of the European Society for the Study of Human Evolution, Zagreb; 2024. 11–15 September 2024.
[55] Mandl I. Collagenases and elastases. In: Advances in enzymology and related areas of molecular biology; 1961. p. 163–264. https://doi.org/10.1002/9780470122686.ch5.
[56] Schweitzer MH, Zheng W, Cleland TP, Goodwin MB, Boatman E, Theil E, Marcus MA, Fakra SC. A role for iron and oxygen chemistry in preserving soft tissues, cells and molecules from deep time. Proc Biol Sci 2014;281:20132741. https://doi.org/10.1098/rspb.2013.2741. 1471-2954 (Electronic).
[57] Velo J. Ochre as medicine: a suggestion for the interpretation of the archaeological record. Curr Anthropol 1984;25(5):674. https://doi.org/10.1086/203205. 674.
[58] Srinivasan DV, Idapalapati S. Review of debonding techniques in adhesively bonded composite structures for sustainability. Sustain Mater Technol 2021;30:e00345. https://doi.org/10.1016/j.susmat.2021.e00345.
[59] Farooq I, Ali S, Al-Saleh S, AlHamdan EM, AlRefeai MH, Abduljabbar T, Vohra F. Synergistic effect of bioactive inorganic fillers in enhancing properties of dentin adhesives—A review. Polymers 2021;13(13):2169. https://doi.org/10.3390/polym13132169.
[60] Fagernäs L, Kuoppala E, Tiilikkala K, Oasmaa A. Chemical composition of birch wood slow pyrolysis products. Energy & Fuels 2012;26(2):1275–83. https://doi.org/10.1021/ef2018836.
[61] Altay L, Sarikanat M, Sağlam M, Uysalman T, Seki Y. The effect of various mineral fillers on thermal, mechanical, and rheological properties of polypropylene. Res Eng Struct Mater 2021;7(3):361–73.
[62] Barczewski M, Mysiukiewicz O, Andrzejewski J, Piasecki A, Strzemięcka B, Adamek G. The inhibiting effect of basalt powder on crystallization behavior and the structure-property relationship of α-nucleated polypropylene composites. Polym Test 2021;103:107372. https://doi.org/10.1016/j.polymertesting.2021.107372.
[63] Ebnesajjad S. Chapter 5 - characteristics of Adhesive Materials. In: Ebnesajjad S, editor. Adhesives technology handbook. second ed. William Andrew Publishing; 2009. p. 63–135. https://doi.org/10.1016/B978-0-8155-1533-3.50008-6.
[64] Parcheta P, Koltsov I, Datta J. Fully bio-based poly(propylene succinate) synthesis and investigation of thermal degradation kinetics with released gases analysis. Polym Degrad Stabil 2018;151:90–9. https://doi.org/10.1016/j.polymdegradstab.2018.03.002.
[65] Sazali N, Ibrahim H, Jamaludin AS, Mohamed MA, Salleh WNW, Abidin MNZ. Degradation and stability of polymer: a mini review. IOP Conf Ser Mater Sci Eng 2020;788(1):012048. https://doi.org/10.1088/1757-899X/788/1/012048.